NTNU

Norwegian University of
Science and Technology

Aeroelastic Instability and Flutter for a 10 MW Wind Turbine

Sigrid Ringdalen Vatne

Master of Science in Energy and Environment
Submission date: June 2011
Supervisor: Ole Gunnar Dahlhaug, EPT
Co-supervisor: Lars Frøyd, EPT

Norwegian University of Science and Technology
Department of Energy and Process Engineering

Norges teknisk-
naturvitenskapelige universitet
NTNU

Fakultet for Ingeniørvitenskap og Teknologi
Institutt for energi- og prosessteknikk

NTNU

EPT-M-2011-55

MASTEROPPGAVE

for
Stud.techn.

Sigrid Ringdalen Vatne
Våren 2011

Aeroelastisk ustabilitet og flutter for en 10 MW vindturbin
Aeroelastic instability and flutter for a 10 MW wind turbine

Bakgrunn

Utviklingen av vindturbiner har vært formidabel i de siste år. Det finnes kommersielt tilgjengelig 5 MW turbiner med diameter over 120 meter. Disse er også installert offshore på bunnfaste installasjoner. Morgendagens turbiner er muligens enda større og kan være flytende. Dette er noe som er tema for forskningssentret NOWITECH. Det jobbes med å utvikle en referanseturbin på 10 MW som skal benyttes i forskningssammenheng på offshore flytende turbiner.

En 10 MW vindturbin er over 150 meter i diameter og har relativt slanke turbin blader. Da det er store krefter som virker på vind turbin bladene så vil disse bøye av noe pga elastisiteten i bladet. Dersom det kommer et vindkast så vil den aerodynamiske lasten endre seg og bladet vil endre utbøyning. Koblingen mellom de aerodynamiske lastene og den elastiske utbøyningen av bladet kan føre til at man får et fenomen som kalles flutter.

Mål
Evaluere om flutter er en utfordring for en 10 MW vindturbin

Oppgaven bearbeides ut fra følgende punkter:
1. Litteratursøk
   a. Gjøre seg kjent med det fysiske fenomenet; flutter
   b. Finne relevante publikasjoner for flutter på vind turbiner

2. Beskrive aeroelastisk ustabilitet og flutter

3. Beregne aeroelastisk ustabilitet og flutter til en 10 MW vindturbin

4. Alle resultatene skal legges tilgjengelig på NTNUs hjemmeside som omhandler fornybar energikilder

Senest 14 dager etter utlevering av oppgaven skal kandidaten levere/sende instituttet en detaljert fremdrift- og eventuelt forsøksplan for oppgaven til evaluering og eventuelt diskusjon med faglig ansvarlig/veiledere. Detaljer ved eventuell utførelse av dataprogrammer skal avtales nærmere i samråd med faglig ansvarlig.

Besvarelsen redigeres mest mulig som en forskningsrapport med et sammendrag både på norsk og engelsk, konklusjon, litteraturliste, innholdsfortegnelse etc. Ved utarbeidelsen av teksten skal kandidaten legge vekt på å gjøre teksten oversiktlig og velskrevet. Med henblikk på lesning av besvarelsen er det viktig at de nødvendige henvisninger for korresponderende steder i tekst, tabeller og figurer anføres på begge steder. Ved bedømmelsen legges det stor vekt på at resultatene er grundig bearbeidet, at de oppstilles tabellarisk og/eller grafisk på en oversiktlig måte, og at de er diskutert utførlig.

Alle benyttede kilder, også muntlige opplysninger, skal oppgis på fullstendig måte. For tidsskrifter og bøker oppgis forfatter, tittel, årgang, sidetall og eventuelt figurnummer.

Det forutsettes at kandidaten tar initiativ til og holder nødvendig kontakt med faglærer og veileder(e). Kandidaten skal rette seg etter de reglementer og retningslinjer som gjelder ved alle (andre) fagmiljøer som kandidaten har kontakt med gjennom sin utførelse av oppgaven, samt etter eventuelle pålegg fra Institutt for energi- og prosessteknikk.
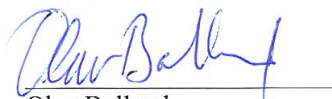
I henhold til "Utfyllende regler til studieforskriften for teknologistudiet/sivilingeniørstudiet" ved NTNU § 20, forbeholder instituttet seg retten til å benytte alle resultater og data til undervisnings- og forskningsformål, samt til fremtidige publikasjoner.

Ett -1 komplett eksemplar av originalbesvarelsen av oppgaven skal innleveres til samme adressat som den ble utlevert fra. Det skal medfølge et konsentrert sammendrag på maksimalt én maskinskrevet side med dobbel linjeavstand med forfatternavn og oppgavetittel for evt. referering i tidsskrifter).

Til Instituttet innleveres to - 2 komplette kopier av besvarelsen. Ytterligere kopier til eventuelle medveiledere/oppgavegivere skal avtales med, og eventuelt leveres direkte til de respektive. Til instituttet innleveres også en komplett kopi (inkl. konsentrerte sammendrag) på CD-ROM i Word-format eller tilsvarende.

NTNU, Institutt for energi- og prosessteknikk

Dato: 3/1 - 2011

Olav Bolland
Instituttleder

Ole Gunnar Dahlhaug
Faglig ansvarlig/veileder

Medveileder: Lars Frøyd

Preface

This Master's thesis is prepared at the Hydro Power Laboratory at the Norwegian University of Science and Technology (NTNU). It is the result of 20 weeks of work.

I would like to thank professor Ole-Gunnar Dahlahaug for the possibility to work with this project. I had not even heard of flutter when he introduced this project to me. Thanks for the supervision and the valuable discussions and support. I would also express my gratitude to my co-supervisor Lars Frøy. He supported me and always had time for my questions.

I would thank Morten Harvig Hansen from Risø DTU. As soon as he heard about my thesis he got interested. He has designed the aeroelastic stability tool, HAWC-Stab2, used in this thesis, and offered valuable advices on the use of this tool and understanding the results. My appreciation to my fellow students at the Hydro Power Laboratory for feedback, support and social gatherings. Finally I would like to thank my boyfriend Sindre Nordmark Olufsen for interesting discussions and much support.

Sigrid Ringdalen Vatne

Trondheim, June 10. 2011

Abstract

The goal of this thesis is to evaluate if flutter is a challenge to a 10 MW wind turbine. Flutter is an aeroelastic instability which occurs due to the interaction between the aerodynamic forces and the elasticity of the blade. Torsional motions of the blade lead to variations in the aerodynamic forces due to changes in the angle of attack of the airfoil. The variation in aerodynamic forces creates flapwise vibration of the blade. When the vibrations of the blades are in an unfavourable phase with the aerodynamic forces, flutter occurs. Flutter may lead to rapidly increasing vibrations of the blade and failure of the blade.

The 10 MW reference turbine from NOWITECH, Norwegian Research Centre for Offshore Wind Technology, was studied. An aeroelastic stability analysis was performed using the aeroelastic stability tool HAWCStab2. It was found that this wind turbine becomes unstable at approximately twice the operational speed of the turbine. The turbine does not experience flutter in normal power producing operation. A simulation in the time domain was also performed, using the aeroelastic tool HAWC2. In a run-away situation, the turbine was found to become unstable with flutter before it reached the run-away speed.

The turbine was then analysed with other blades. A softer blade and a stiffer blade were studied. The soft blade was found to become unstable at 1.8 times the operational speed of the turbine. The stiff blade was found to become unstable at around 2.5 times the operational speed. The stiff blade was the only blade where the turbine was able to reach the run-away speed without experiencing instabilities.

Sammendrag

Målet med denne oppgaven er å evaluere om flutter er en utfordring for en 10 MW vindturbin. Flutter er en aeroelastisk ustabilitet som oppstår på grunn av en kobling mellom de aerodynamiske kreftene og elastisiteten i bladet. Torsjon av bladet kan endre de aerodynamiske krefter på grunn av endret angrepsvinkel. Dette kan videre påvirke utbøyingen av bladet. Når vibrasjonene fra bladene er i ugunstig fase med de aerodynamiske kreftene, absorberer bladene energi fra vinden pumpes energi fra vinden inn i bladene og flutter oppstår. Flutter kan føre til vibrasjoner med raskt økende amplitude som kan ødelegge vindturbinen.

Vindturbinen som studeres i denne oppgaven er NOWITECH sin 10 MW referanse turbin. En stabilitetsanalyse ble utført ved hjelp av det areoelastiske analyseprogrammet HAWCStab2. Resultatene fra denne analysen viste at vindturbinen ble ustabil ved omtrent dobbel så høy rotasjonshastighet som driftshastigheten på turbinen. Turbinen er ut fra dette ikke utsatt for flutter i normal drift. En simulering i tidsdomenet ble deretter gjennomført ved hjelp av et aeroelastisk simulerinsgsprogram, HAWC2. En rusingssituasjon ble studert, hvor rotoren mister motmomentet fra generatoren og akselererer opp i rotasjonshastighet. Flutter ustabilitet inntraff før turbinen nådde en konstant rotasjonshastighet.

Det ble også gjennomført en analyse hvor andre blader ble brukt på turbinen. En turbin med mykere blad og en med stivere blad ble studert. Det myke bladet ble ustabilt ved 1.8 ganger driftshastigheten. Det stive bladet ble ustabilt ved 2.5 ganger driftshastigheten. Det stive bladet var det eneste bladet i denne analysen som nådde konstant hastighet i en rusingssituasjon uten at ustabilitet oppsto.

Contents

List of Figures

List of Tables

Nomenclature

Symbols

α	Angle of attack [deg]
β	Pitch angle [deg]
ζ	Damping ratio [-]
θ	Torsional angle [deg]
κ	Timoshenko shear coefficient [-]
κ	Aerodynamic stiffness [-]
λ	Eigenvalue
ρ	Air density [kg/m^3]
ρ_B	Density of the blade [kg/m^3]
ϕ	Azimuth angle [deg]
Ω	Rotational speed [rad/s]
ω	Modal frequency [Hz]
A	Area [m^2]
a_{CG}	Fraction of chord length between EA and CG [m]
a_{AC}	Fraction of chord length between EA and AC [m]
C_L, C_D, C_M	Lift, drag and moment coefficient [-]
C'_L	Gradient of lift coefficient with respect to angle of attack [1/deg]
$\mathbf{C}$	Damping matrix
c	Blade chord length [m]
D	Aerodynamic drag [N]
d	Damping coefficient [Ns/m]
E	Young modulus of elasticity [Pa]
f	Frequency [Hz]
G	Shear modulus [Pa]
$\mathbf{G}$	Gyroscopic matrix
h	Flapwise deflection [m]
I	Moment of inertia [m^4]
J	Polar moment of inertia [m^4]
$\mathbf{K}$	Stiffness matrix
k	Reduced frequency [-]
k_i	Stiffness coefficient [N/m]

L	Aerodynamic lift [N]
$\mathcal{L}$	Lagrangian operator
$\mathbf{M}$	Mass matrix
M	aerodynamic moment [Nm]
m	Mass [kg]
q	Applied load per unit length [N/m]
$\mathbf{Q}$	Applied forces [N]
r_{CG}	Radius og gyration [m]
t	Time [s]
$\mathbf{u}$	Node deformation vector
W	Relative wind speed [m/s]
x	Direction outward on blade [m]
y	Edgewise deflection [m]
z	Aerodynamic state

Subscripts

f	Flapwise
e	Edgewise
t	Torsional
k	Blade number
E	Effective

Acronyms

DoF	Degree of Freedom
BEM	Blade Element Momentum method
TSR	Tip Speed Ratio
EA	Elastic Axis
CG	Center of Gravity
AC	Aerodynamic Centre

Chapter 1

Introduction

The development of wind turbines has been enormous the last decade. As the demand for renewable energy sources increases, wind turbines are an attractive opportunity. To enhance the energy capture per unit wind turbine, the wind turbine size is increasing. Wind turbines are also being planned offshore, which enables even bigger wind turbines, as there are no people near enough to complain about the size and the noise. NOWITECH, the Norwegian Research Centre for Offshore Wind Technology, plan to develop a 10 MW floating reference wind turbine, to study how such a turbine behaves. The turbine is planned to have a rotor diameter of 140 m.

The rotor blades of big wind turbines are long and slender, with large forces on the blades. These blades bends and twist due to the elasticity of the blades. The blade bending affects the aerodynamic forces on the blades by changing the angle of attack. As a result an aeroelastic instability known as flutter may occur. Flutter is a well-known phenomenon from the aircraft industry. It happens when an unfavourable coupling between aerodynamic forces and flapwise and torsional vibrations of the blade occur at high wind speeds. Flutter leads to rapidly increasing blade vibrations and may ultimately lead to failure. No failure due to flutter has yet been reported on commercial wind turbines, but it may become a problem with the increased size of the wind turbine. To be sure that the NOWITECH reference turbine is not subject to flutter near its operational area, the aeroelastic stability of this turbine is studied in this thesis. The theory for computing the critical flutter speed is studied. The stability of the wind turbine is investigated through aeroelasic stability analyses and time-domain simulations. The time domain analysis is performed using the aeroelastic simulation tool HAWC2, and the aeroelastic stability analysis was performed in HAWCStab2. Three different blade configurations with different stiffness of the blade will be studied to find out how this affects the flutter limits.

Chapter 2

Literature Survey

2.1 Aeroelasticity

Aeroelasticity is the study of how aerodynamic forces affect elastic bodies. The aerodynamic forces can lead to a deformation of the elastic body, which consequently can result in changed aerodynamic forces. This interaction between the deformation of the body and aerodynamic forces may lead to complex problems.

There are several types of constructions where aeroelasticity have to be considered. Bridges and buildings are exposed to forces from the wind. Aircrafts and wind turbines are exposed to the wind and dependent on forces from the wind to operate as intended. Subsea structures are exposed to forces from waves and currents (hydroelasticity). In the human body, several organs are dependent on the correct collaboration between the flow and the elastic tissue. An example of this is how the hearts pumps blood through the body.

The steady aeroelastic deformation of a body is often relevant and has to be calculated. For a wind turbine it is important that the steady deflection of the blades due to the wind load does not result in the blades hitting the wind turbine tower. Aeroelastic instabilities may be just as disastrous, and more difficult to calculate.

When aeroelastic instabilities occur, the phase difference between the motions of the structure and the aerodynamic forces becomes such that the structure absorbs energy from the air. The aerodynamic forces pump energy into the structure, leading to vibrations with increasing amplitude. In the worst case scenario this can lead to failure of the structure. The most famous accident due to aeroelastic instability is the collapse of the Tacoma Narrows Bridge, also known as "Galloping Gertie" in Washington, US, in 1940. A photo of the vibrations on the bridge prior to its failure, is shown in figure 2.1. The failure happened at a wind speed far below what the bridge was designed to withstand without vibrations. The failure

of the bridge is generally believed to be due to stall flutter [5]. Stall flutter is an aeroelastic instability which occurs when the structure is in stalled conditions.
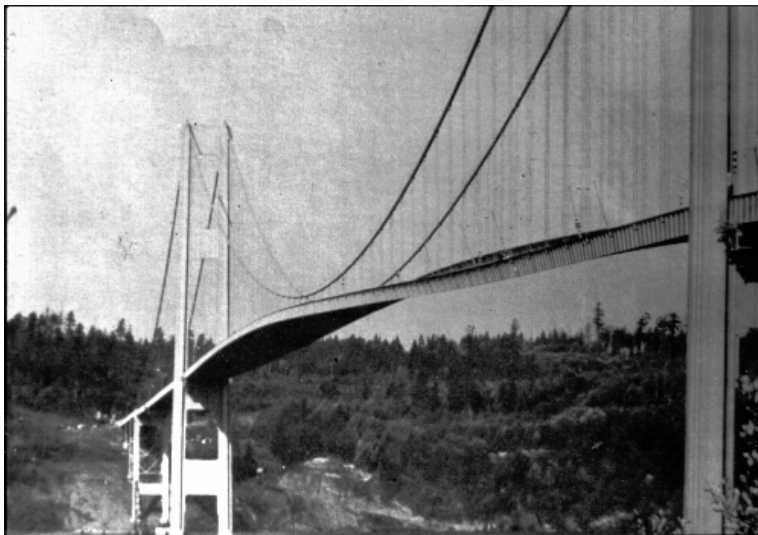
Figure 2.1: Vibrations of the Tacoma Narrows Bridge prior to its breakdown. From [1]

In this thesis the focus is on classical flutter. Classical flutter is an aeroelastic instability involving coupling of the torsion and the deflection of the body. When classical flutter occurs, it rapidly creates violent vibrations, and potentially failure of the structure. Classical flutter is known from aircraft and civil engineering and may also occur in the human body. No commercial wind turbines have so far been reported to fail due to classical flutter [2]. Subsequently classical flutter will be denoted as "flutter", which is not to be confused with stall flutter.

2.2 Flutter

Flutter is an aeroelastic instability involving 2 degrees of freedom (DoF), one flapwise and one torsional. The definition of the DOFs is found in chapter 3.1. The torsional structural mode (usually the first mode) couples with a flapwise bending mode in a flutter mode through the aerodynamic forces. The aerodynamic forces lead to torsion of the structure. The torsion changes the angle of attack and thus the aerodynamic lift force [2]. Flutter occurs when the change of angle of attack due to torsion changes the lift in an unfavourable phase with the flapwise bending. Flutter causes violent vibrations with rapidly growing amplitude. The flutter mode has a highly negative damping which can not be compensated by the structural damping. Flutter only happens above a certain relative wind speed on the structure, known as the critical flutter speed. The definition of the critical flutter speed

4

limit, is the wind speed at which the aeroelastic system will oscillate harmonically without further excitation after an initial disturbance [5].

Even though no wind turbines have failed due to flutter, it is important to investigate the possibility of flutter on wind turbines. With the rise of bigger wind turbines, flutter may become a dimensioning criterion. Due to the increasing flexibility of the blade and the increased relative velocity at the blade tip, bigger wind turbines tend to become more prone to flutter.

From studies of aircraft wing flutter, it is assumed that a wind turbine has risk of flutter if the following criteria is met [2]:

1. *Attached flow.* The flow needs to be attached to the blade to ensure that a nose-up blade torsion leads to increased lift.

2. *High tip speeds.* A high tip speed leads to a sufficiently high relative wind speed, which is needed for the wind to have high energy in the aerodynamic forces.

3. *Low stiffness.* The natural frequencies of the torsional and flapwise bending mode must be sufficiently low for them to couple and create flutter.

4. *Center of mass aft of the aerodynamic centre.* An aft centre of gravity compared to the aerodynamic centre ensures the right phase difference between the flapwise and torsional components of flutter

Other parameters such as the air-blade mass ratio, blade aspect ratio, material damping and structural bending-torsion couplings also influence the critical flutter limit.

To study if a wind turbine is prone to flutter, a stability analysis of the wind turbine has to be performed. In chapter 3, the methods used for performing such a stability analysis are discussed.

Figure 2.2: Example of a blade flutter mode over one period of oscillations on a wind turbine blade [2]

2.2.1 Flutter on aircrafts

Most of the theory for predicting the critical flutter speed has been developed for aircrafts. Through history several aircrafts have crashed due to flutter, and consequently flutter on aircraft wings is extensively studied. On an aircraft wing not only the coupling between the torsion and flapwise degrees of freedom on the

blade can result in flutter, also the motion of the aileron relative to the rest of the wing can cause flutter. On a wind turbine this is not a problem, as there are no ailerons or similar flaps on the blades.

The earliest study of flutter on aircrafts is the studies made by Lancheter, Bairstow and Fage in 1916 in connection with flutter on a Handley Page Bomber, as described by Fung [5]. The main development of flutter analysis started after the development of non-stationary airfoil theory, by Kutta and Jukowski around 1905. In 1934 Theodorsen's exact solution of a harmonically oscillating wing with a flap was published [6]. Theodorsen was born in Norway and graduated from NTH with a degree in mechanical engineering, but emigrated to the US and worked for NACA, the National Advisory Committee for Aeronautics. His work is an important part of the foundation of flutter calculations. It applies unsteady aerodynamics and the frequency domain, to calculate the critical flutter limit. After this, the theory of flutter was further developed and the tools became better and more suitable for faster calculations. To study a three dimensional wing with more than 2 degrees of freedom (DoF), Galerkins method was applied together with strip theory of aerodynamics. The flutter phenomenon was also experimentally investigated. In 1955 Fung published a book on aeroelasticity, which includes most fields of aircraft aeroelasticity [5]. This book is still highly relevant and includes a lot of theory on flutter prediction. As airplanes began to be constructed to operate in transonic and supersonic flight, the flutter prediction had to be developed to handle cases with compressibility effects. With the increasing computational power of computers the last decades, Computational Fluid Dynamics (CFD) can also be to model unsteady aerodynamics. It is then coupled with the structural computations, like Finite Element Method (FEM), to calculate the aeroelastic effects. This is very computational intensive method.

2.2.2 Flutter on wind turbines

There has so far been little research on wind turbine flutter. A plausible reason for this is that no wind turbines have yet been subject to flutter. Smaller wind turbines do not experience flutter due to the stiff blades with low tip speed. For rotor blades in the size of 10 m, the critical flutter speed has been calculated to be approximately 5 times the operating speed of the wind turbine [7]. For MW-sized wind turbines, the flutter speed is found to be about twice the operational speed, by among others Hansen [2]. In several studies, like Lobitz [8], it was found that it was the second flapwise mode and the first flapwise blade mode which coupled in flutter. But Hansen [2] showed that for the NREL 5 MW turbine, the third flapwise mode couples with the first torsional blade mode.

Parts of the theory on aircraft flutter analysis can be adapted to analyses of flutter on wind turbines. One of the first linear stability tools able to analyze wind turbine stability was ARLIS from 1984 [9]. It was originally designed for rotorcrafts, but could also be used to analyse wind turbines. As wind turbines, especially stall controlled ones, are more prone to stall induced vibrations than to classical flutter,

stall induced vibrations was investigated at an earlier time. An early attempt to model edgewise vibrations on wind turbines was made under the European research program STALLVIB in 1998 [10]. The main outcome of this project was the fact that the edgewise vibrations are caused by negative aerodynamic damping. The aerodynamic damping of the edgewise vibrations was approximated by the work done by the aerodynamic force on the blade over one period of oscillation. The European VISCEL project [11] investigated a typical blade section to study stall induced vibrations. Unsteady Navier-Stokes treatment of the aerodynamics was performed in the time-plane. It was concluded that a linear model is conservative when evaluating instabilities. Even though these tools were developed to study stall-induced vibrations, some of them can also be used to study classical flutter.

New stability tools were developed under the European DAMPBLADE project [12], based on single blade analyses. Standard structural modelling was combined with the Blade Element Momentum method (BEM) and unsteady aerodynamic models. The tools were used to perform eigenvalue analyses. The main issue in developing new tools for stability analysis has been the linearization and state-space formulation of the aerodynamic models [3]. Another major outcome of the DAMPBLADE project was the development of a theory to model not only the aerodynamic damping, but the structural damping of a wind turbine blade as well.

It is also possible to run aeroelastic simulations in the time-plane. Time domain simulations does not give all the information of an eigenvalue analysis, but can be useful. The most detailed description of the turbine response is given by such time-domain simulations, as it can implement non-linearities better than eigenvalue analyses. Simulation codes useful for performing a time-domain simulations may be HAWC2 [13], by Risø DTU, National Laboratory for Sustainable Energy in Denmark and FAST [14] by NREL, National Renewable Energy Laboratories in the United States. Another possible method for studying aeroelastic instabilities is using CFD to model the aerodynamics, and then couple it with the structural model. In the KNOWBLADE European research project, tools for isolated blade analysis using a Navier-Stokes aerodynamic analysis were developed.

Single blade analyses shows that the predicted critical flutter speed is lower when using quasi-steady aerodynamics instead of unsteady aerodynamics. This was shown by Lobitz [8] for a MW-sized blade. Lobitz [15] also confirmed that the critical flutter speed decreases when the centre of mass moves towards trailing edge, using a single blade analysis. Similarly the critical flutter speed decreases when the ratio of the natural frequencies of the flapwise and the torsional blade modes was reduced. The same study showed that the flutter speed compared to the operational speed should not change when the blade is scaled. The different design requirements with increasing blade size are what may change the critical flutter speed for bigger blades.

The European Union founded project UPWIND deals, among other issues, with non-linear modelling of blades and the effects of including such non-linearities. A steady state deflection of the blade results in geometrical non-linearities, which

have to be taken into account. Kallesøe [16] used a single blade analysis, with a non-linear blade model to study the effect of large bending deflections on blade flutter limits, on the NREL 5 MW reference turbine. He found no significant change of the flutter limit on the rotor speed due to a steady state flapwise blade deflection. But a negative damping of the first edgewise bending mode was found. This is assumed to be due to the coupling of the edgewise bending mode with blade torsion, which causes a change of the effective direction of the blade vibrations. Hansen [17] showed that backward swept blade creates torsion towards feathering for downwind flapwise deflection in the first flapwise blending mode. The critical flutter speed was found to decrease for backward swept blades.

The single blade analysis may be unconservative as modes of the complete wind turbines contain significant blade-to-blade and blade-to-tower interactions. Under the STABCON European research program [18], aeroelastic tools for determining the aeroelastic stability of the entire wind turbine was developed, among others by Risø [3], Sandia National Laboratories in the United States [19] and ECN Energy Research Center of the Netherlands [20]. Methods developed at various European institution were cross-validated using experimental data for a variable speed, pitch regulated wind turbine. The aeroelastic stability program used in this study, HAWCStab [3], was developed under the STABCON project. It performs a full stability analysis of the entire wind turbine. A new version of this tool has been developed by Hansen, but only the work on the blades has been published [17]. This new version, HAWCStab2, is able to calculate the nonlinear blade coupling effects on flutter limit, and thus a more correct flutter speed for blades with a large steady flapwise deformation.

Some state-of-the-art issues in flutter analysis, which need to be investigated is [2]:

- *Flutter experiments.* No experimental data are currently available for validation of the flutter limits predicted for conventional three-bladed wind turbines using the aeroelastic stability tools.

- *Near wake effects on flutter limits.* This is a unsteady aeroelastic effect which arises due to variations in the trailing vorticity of the near wake as the blade vibrates. The effect is similar to the near wake effect modelled by Theodorsen aerodynamics. The near wake effect depends on the radial distribution of the lift and is largest near the tip.

- *Flutter limits for yaw misaligned flow.* It should be investigated if a wind turbine in large yaw misalignment with the wind may experience flutter as a part of the blade rotation where the blade meets the incoming wind with higher relative speed.

- *Pitch-torsion coupling in flutter modes.* The torsional flexibility of the pitch system due to compressibility of the hydraulic liquids or free play in the electromechanical pitch gear, is assumed to affect the flutter limits.

- *Active damping using trailing edge flaps.* Active suppression of flutter using trailing edge flaps is a research technology on aircraft wings, which could be

directly applicable for wind turbines.

- *False linear flutter limits due to large nonlinearities.* Large nonlinearities may change the type of the flutter instability. The linear stability analysis may thus predict a too high flutter limit.

2.3   Stall induced vibrations

Stall induced vibrations denotes an aeroelastic instability which can occur on blades in stalled conditions. It is also known as stall flutter. On wind turbines stall flutter mainly occurs on stall-regulated turbines, as they are designed to operate in stalled conditions at high wind speeds. Stall induced vibrations are generally less violent than vibrations due to classical flutter. Stall induced vibrations have been experienced by several wind turbines. As a result of this, more research has been performed on stall induced vibrations, than on classical flutter, for example by Hansen [21] and Chaviarpoulos [11]. Stall induced vibrations are often a combination of edgewise and flapwise vibrations. The parameter which dominates the risk of stall-induced vibrations are, according to Hansen [2], the airfoil characteristics, the direction of the vibrations and the structural damping. If the blades have airfoils with abrupt stall characteristics, the risk of stall flutter increases. The directions of blade vibrations depend on the entire turbine dynamics and some of these gives a higher risk of stall induced vibrations. The structural damping is important because it can compensate the slightly negative aerodynamic damping due to the stall-induced vibrations. In classical flutter the negative aerodynamic damping is much higher and the structural damping can not compensate.

As stall-induced flutter is mainly an issue on stall-regulated turbines, and the turbine in question is pitch-regulated, the main focus in this thesis is classical flutter.

It is also possible for other modes to couple to an aeroelastic instability. This may be due to an unfavourable coupling of eigenfrequencies. Such vibrations are not common, and are not expected to occur for a wind turbine.

Chapter 3

Methods for Aeroelastic Instability Calculations

In this chapter the basic theory of aeroelasticity, and flutter calculations are presented. First the coordinate systems and terms used are presented. Then the basic structural dynamics and aerodynamics used in the aeroelastic calculations are derived. To understand the flutter dynamics, first the qualitative aeroelastic considerations of single sections are discussed. Then the aeroelastics of an aircraft is presented, leading to the aeroelastics calculations used in aeroelastic stability tools.

3.1 Degrees of freedom and coordinate systems

To avoid confusion, the same terms are going to be used on all types of blades, wind turbine blades, aircraft wings or a typical section of a blade. The terms used corresponds to the terms used by Hansen [2].

On a single blade, the degrees of freedom (DoF) important for the aeroelastic analysis are denoted flapwise, edgewise and torsion. At zero pitch of the wind turbine blades, flapwise correspond to the out-of-rotor-plane motion, whereas edgewise corresponds to in-plane motions at the blade tip. The DoFs are shown in figure 3.1.

The DoFs on a complete wind turbine can be found in figure 3.2. The tower may bend in fore-aft or side-to-side direction, which is parallel to or perpendicular to the wind direction respectively. Fore-aft motion of the tower leads to tilt motion of the nacelle, and side-to-side motion of the tower lead to a roll motion of the nacelle. Torsion of the tower results in a yaw motion of the nacelle. A yaw motion is also used to align the rotor with the wind direction. When the shaft rotates, the rotor blades rotate in the azimuthal direction. The azimuth angle is assumed to

(a) Flapwise   (b) Edgewise   (c) Torsion
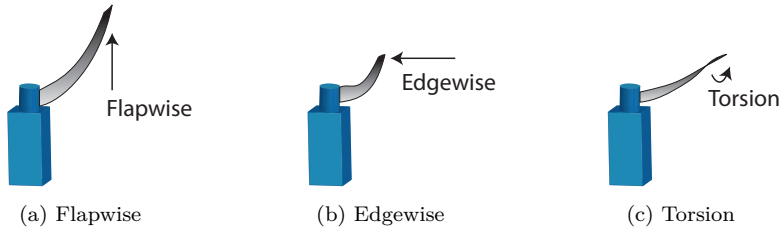
Figure 3.1: Degrees of freedom on the blade, modified from Hansen [2]

be zero when the blade is in downward position. As the wind turbine in question is pitch regulated, the blades can pitch about the pitch axis to regulate the angle of attack of the wind and thus the power output from the turbine.
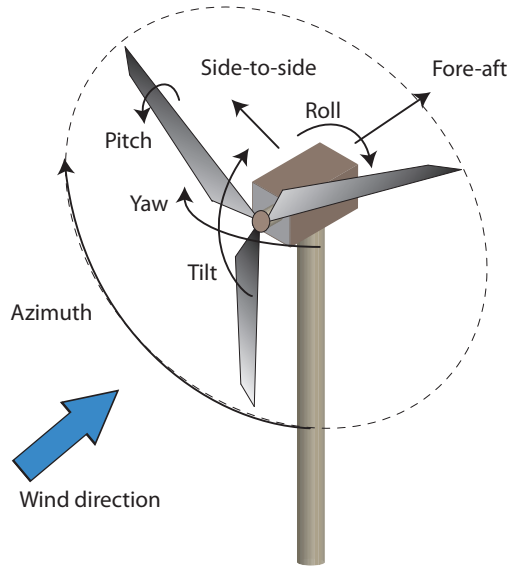
Figure 3.2: Tower coordinate system

The coordinate system of a typical section of a blade is found in figure 3.3

The typical section has three DoFs, flapwise translation $h(t)$, edgewise translation, $y(t)$ and rotation $\theta(t)$ about the elastic axis (EA). It can also have a DoF describing the edgewise direction, $y(t)$. The elastic axis is a length $c \cdot a_{CG}$ in front of the centre of gravity (CG). c is the chord length and a_{CG} is the fraction of the length between the elastic axis and the centre of gravity and the chord length. The aerodynamic lift, L is defined at the aerodynamic centre (AC), in a distance $c \cdot a_{AC}$ in front of
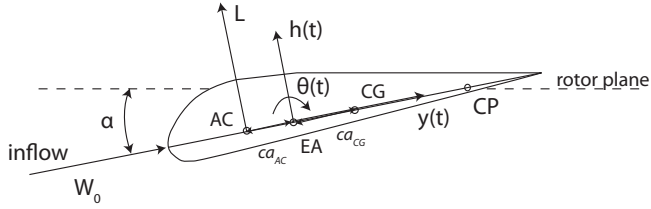
Figure 3.3: Coordinate system on a typical section of the blade

the torsional point. At this point is also possible to define the aerodynamic drag, D and moment, M. The aerodynamic centre (AC), usually lies at around 1/4 of the chord length. The angle of attack, α is defined at the collocation point (CP), at three quarter of the chord length. This is to capture the effect of torsional velocity $\dot{\theta} \neq 0$. It is also possible to define the angle of attack at the elastic axis. The incoming relative wind speed is denoted W_0.

3.2 Structural dynamics

The structural dynamics in aeroelasticity calculations are often based on beam theory. The standard beam theory is linear and known as the Euler-Bernoulli beam theory. The relationship between the applied load per unit length, q, and the deflection, h, is described with the following equation, where x is the direction of the beam:

$$\rho_B A \frac{\partial h^2}{\partial^2 t} + \frac{d^2}{dx^2}\left(EI\frac{d^2 h}{dx^2}\right) = q(x,t) \qquad [N/m] \tag{3.1}$$

Another common method is the Timoshenko beam theory [22]. This model takes into account shear deformation and rotational inertia effects. The governing dynamic equations using in beam model are:

$$\begin{aligned} \rho_B A \frac{\partial h^2}{\partial^2 t} &= \frac{d}{dx}\left[\kappa A G \left(\frac{dh}{dx} - \varphi\right)\right] + q(x,t) \qquad [N/m] \\ J \frac{d^2 \varphi}{dx^2} &= \frac{d}{dx}\left(EI\frac{d\varphi}{dx}\right) + \kappa A G \left(\frac{dh}{dx} - \varphi\right) \qquad [-] \end{aligned} \tag{3.2}$$

In both equations, E is the Young's elastic modulus, x is the direction outward on the beam, and I is the moment of inertia of the beam. φ is the slope of the beam due to bending, A is the area of the beam and G the shear modulus of the beam. κ is the Timoshenko shear coefficient, which varies with the geometry of the beam. If the shear modulus of the beam approaches infinity and rotational inertia effects are neglected, the Timoshenko beam theory converges towards Euler-Bernoulli beam theory.

13

To calculate how the structures react to external forces, the equations of motion of the structure has to be known. To derive the equations of motion for a structure, it is possible to use Lagrange's equation:

$$\frac{d}{dt}\left(\frac{\partial \mathcal{L}}{\partial \dot{x}_j}\right) - \frac{\partial \mathcal{L}}{\partial x_j} = Q_j \qquad [N] \tag{3.3}$$

where $\mathcal{L}$ is the Lagrangian operator: $\mathcal{L} = \mathcal{T} - \mathcal{V}$. $\mathcal{T}$ is the kinetic energy of the system and $\mathcal{V}$ is the potential energy. x_j is the independent coordinates and Q_j are the generalized forces.

After a examination of the system and forces at hand, and possibly Lagrange method, the equations of motion can then be found:

$$\mathbf{M\ddot{x}} + \mathbf{C\dot{x}} + \mathbf{Kx} = \mathbf{Q} \qquad [N] \tag{3.4}$$

where $\mathbf{M}$ is the mass matrix, $\mathbf{C}$ is the damping matrix, $\mathbf{K}$ is the striffness matrix and $\mathbf{Q}$ is the external forces. There are several ways to write out the equations of motion for a wing. In Fung [5] the equations of motion for a cantilever wing are described, using Euler-Bernoulli beam theory and two DoF, as:

$$\begin{aligned} \frac{\partial^2}{\partial x^2}\left(EI\frac{\partial^2 h}{\partial x^2}\right) + m\frac{\partial^2 h}{\partial t^2} + mca_{CG}\frac{\partial^2 \theta}{\partial t^2} + L = 0 \qquad [N] \\ \frac{\partial}{\partial x}\left(GJ\frac{\partial \theta}{\partial x}\right) - I_\alpha\frac{\partial^2 \theta}{\partial t^2} + mca_{CG}\frac{\partial^2 h}{\partial t^2} + M = 0 \qquad [Nm] \end{aligned} \tag{3.5}$$

L is the aerodynamic lift and M the aerodynamic moment. The equations of motion can also be written using stiffness and damping coefficients. The structure is then modelled as a spring-mass-damper system, with the springs and dampers as shown in figure 3.4. It is also possible to model the edgewise motion with a spring and a damper.
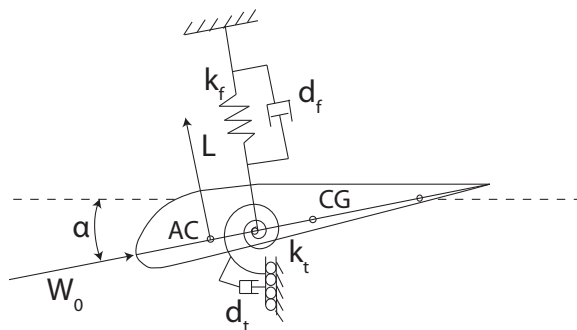
Figure 3.4: A blade element modeled with springs and dampers in flapwise and torsional direction

When studying aeroelastic instability on a blade it may be useful to express the stiffness as function of the uncoupled modal frequencies, ω. The subscript f denotes flapwise and t denotes torsional direction.

$$k_f = \omega_f^2 m, \quad k_t = \omega_t^2 m \qquad [N/m] \tag{3.6}$$

For a blade section of a wind turbine with only 2 DoFs, flapwise and torsional, where structural damping is neglected, the linear equations of motion can, using this, be written as [5]:

$$\begin{aligned}
m\ddot{h} - mca_{CG}\ddot{\theta} + k_f h &= L \qquad [N] \\
-mca_{CG}\ddot{h} + mc^2(r_{CG}^2 + a_{CG}^2)\ddot{\theta} + k_t\theta &= ca_{CG}L \qquad [Nm]
\end{aligned} \tag{3.7}$$

where $r_{CG} = \frac{I}{m \cdot c}$ is the radius of gyration normalized whit the chord length c, and k_f and k_t is the flapwise and torsional stiffness respectively.

To better describe the motions of a blade section the edgewise DoF has to be considered, in addition to the flapwise and torsional DoFs. A lower order model of a blade section with both spring and dampers using all 3 DoFs can be found in Kallesøe [23]. The method is an extension from Hodges-Dowell's partial differential equation for helicopter wings.

The damping of the aeroelastic system is mainly due to the aerodynamic forces. But also the structure dampens oscillations. The structural damping of the wind turbine blade was studied in the DAMPBLADE project [12], where tools for modelling the damping was developed, as well as new types of more damped composite blades.

Some new approaches for increased damping of composite blades which were investigated in the DAMPBLADE project was [12]:

- Using composites of high-damping polymer matrices.

- Tailoring ply orientation, fibre volume fraction and stacking sequence for optimal damping capacity.

- Using sandwich composite laminates with shearly damped polymer foam cores.

3.3 Aerodynamics

The aerodynamic lift and drag forces arise as the wind around an airfoil creates different pressure at the upper and lower side of the airfoil. The lift force can be expressed as a function of the lift coefficient as described in equation 3.8. For quasi-steady flows the lift coefficient is solely a function of the angle of attack $C_L = C_L(\alpha)$. For unsteady flow, the lift coefficient is also dependent on earlier

flow conditions. There also exists corresponding equations of the drag and pitching moment.

$$L = \frac{1}{2}\rho c W^2 C_L \qquad [N] \qquad (3.8)$$

To simplify the aerodynamic calculations, the strip assumption is often used. This assumption states that the aerodynamic forces on a section or strip of the blade are only determined by the angle of attack at this section, and not dependent of the forces on the neighbouring sections.

For airplanes, the traditional method for computing lift and drag forces on a wing is the method of circulation, developed by Kutta and Jukowzki. A description of the steady theory can be found in Bertin [24] and Fung [5]. A steady thin airfoil can be modelled with several vortices, each with a circulation strength, γ. For an unsteady flow, the model of the airfoil consists of both free and bound vortices. The vortices is shed at the trailing edge and carried downstream with the flow.

For wind turbines the Blade Element Momentum method (BEM) is a much-used method for calculating the aerodynamic forces. The derivation of BEM can be found in Manwell [25]. The BEM is a quasi steady method, based on the strip assumption, which combines the momentum method with the blade element method. BEM can be extended with models to handle some of the effects of unsteady flows. The most used models for describing the unsteady effects are the Beddoes-Leishman dynamic stall model, and the ONERA Lift and Drag dynamic stall model.

When Theodorsen derived a method of deriving the critical flutter speed, he developed a theory to handle unsteady aerodynamic effects. The method is based on potential flow theory and the Kutta condition. It includes a dynamic model of the trailing near wake [6]. The model was derived for a blade simultaneously pitching and plunging in a oscillatory fashion described by

$$h = h_0 e^{i\omega t} \quad [m], \qquad \theta = \theta_0 e^{i\omega t} \quad [rad] \qquad (3.9)$$

where h_0 and α_0 are complex constants, and ω the frequency of the oscillations. According to Theodorsen the unsteady lift of an airfoil can be described as [8]:

$$L = \pi \rho W^2 c \left(\frac{i\omega C(k)}{W} \dot{h} + C(k)\theta_0 + [1 + C(k)(1 - 2a)]\frac{i\omega c}{4W}\theta_0 - \frac{\omega^2 c}{4W^2} h_0 + \frac{\omega^2 c^2 a}{8W^2}\theta_0 \right) \qquad [N]$$

$$(3.10)$$

$C(k)$ is the Theodorsen's function of the reduced frequency $k = \omega c/W$ and a is the fraction of the chord between the elastic axis and the mid-chord.

An unsteady aerodynamic state space model, based on the Beddoes-Leishman dynamic stall model, was suggested by Hansen [26]. Dynamic stall is an unsteady
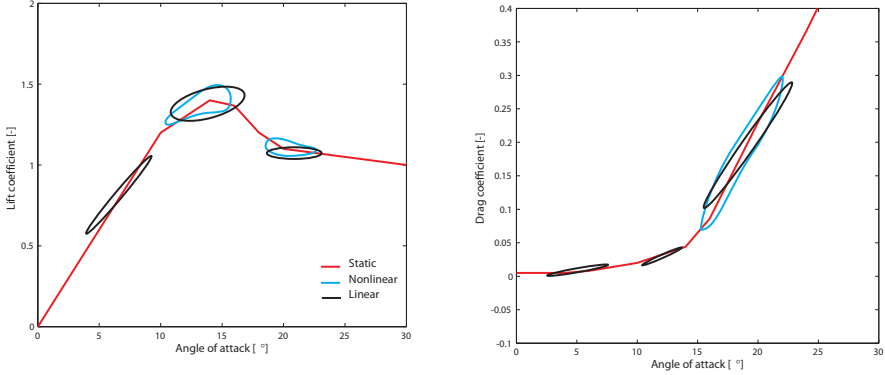
Figure 3.5: Comparision of dynamic stall and linear and nonlinear dynamic stall model. Modified from [3]

aerodynamic effect which is characterized by the hysteresis of the lift and drag polars with respect to the angle of attack. Variations in blade loading change the vorticity trailed into the rotor wake, and the full effect of these changes takes a finite time to affect the induced velocity field. This leads to a time delay of the aerodynamic lift and drag. The model includes the dynamic effects of the near wake from Theodorsen theory and the effect of trailing edge separation in stall on the aerodynamic lift, drag and moment coefficients. The model uses four aerodynamic states to describe the dynamics of the unsteady forces. States z_1 and z_2 model the time-lags in the near wake effect. States z_3 and z_4 describes time-lags in the effect of trailing edge separation. The aerodynamic state equations are:

$$\dot{z}_1 + T_u^{-1}\left(b_1 + c\frac{\dot{W}}{2W^2}\right)z_1 = b_1 A_1 T_u^{-1}\alpha_{3/4} \qquad [1/s] \tag{3.11a}$$

$$\dot{z}_2 + T_u^{-1}\left(b_2 + c\frac{\dot{W}}{2W^2}\right)z_2 = b_2 A_2 T_u^{-1}\alpha_{3/4} \qquad [1/s] \tag{3.11b}$$

$$\dot{z}_3 + T_p^{-1}z_3 = T_p^{-1}C_L'(\alpha_E - \alpha^0) + \frac{T_u\pi}{T_pW}\left[W\dot{\alpha} + \dot{W}\alpha - (l_{EA} - \frac{c}{2})\ddot{\alpha} - \ddot{h}\right] \qquad [1/s] \tag{3.11c}$$

$$\dot{z}_4 + T_f^{-1}z_4 = T_f^{-1}f^{st}\left(z_3/C_L' + \alpha^0\right) \qquad [1/s] \tag{3.11d}$$

$T_u = c/2W$ is a normalized time constant and T_p, T_f, b_1, b_2, A_1 and A_2 are different time lags. $f^{st}(\alpha)$ is the function which describes the static trailing edge separation point.

To create the final aerodynamic equations of motion, the aerodynamic equations have to be coupled with the structural dynamics. An easy way is to use the aerodynamic forces as external forces in the structural equations from chapter 3.2. If

aerodynamic state equations are used, these have to be implemented to the structural dynamics. If the goal is to perform an eigenvalue analysis, the equations have to be linearised. The standard approach is to linearise the aerodynamic equations and the structural equations of motion separately, before they are coupled.

3.4 Flutter instability mechanisms

In this section an example of an eigenvalue calculation is shown. The calculation is performed to show the quantitative mechanisms which influence the critical flutter speed. The calculations in this section include many simplifications, to make the equations readable. The calculations in this section is from Hansen [2].

To calculate the critical flutter limit, the typical blade section from figure 3.3 is considered. To simplify the system, the typical section is assumed to have only two degrees of freedom, torsional, $\theta(t)$ and flapwise, $h(t)$. The section is exposed to quasi-steady lift forces without apparent mass terms. As discussed in chapter 3.2 the linear equations of motion can be derived as:

$$
\begin{aligned}
m\ddot{h} - mca_{CG}\ddot{\theta} + k_f h &= L \qquad [N] \\
-mca_{CG}\ddot{h} + mc^2(r_{CG}^2 + a_{CG}^2)\ddot{\theta} + k_t \theta &= ca_{CG}L \qquad [Nm]
\end{aligned}
\tag{3.12}
$$

where $r_{CG} = \frac{1}{c}\sqrt{I/m}$ is the radius of gyration normalized with the chord length c, and k_f and k_t are the flapwise and torsional stiffness respectively.

The quasi-steady aerodynamic lift per unit-length can be described as:

$$
L = \frac{1}{2}\rho c W^2 C_L(\alpha) \qquad [N]
\tag{3.13}
$$

where the relative speed, W and the angle of attack α are here defined as:

$$
\begin{aligned}
W &= \sqrt{W_0^2 + \dot{h}^2} \qquad [m/s] \\
\alpha &= \arctan\left(\frac{W_0\sin\theta - \dot{h} - c\left(\frac{1}{2} - a_{AC}\right)\dot{\theta}}{W_0\cos\theta}\right) \qquad [rad]
\end{aligned}
\tag{3.14}
$$

When linearizing equation 3.13 about $\theta = \dot{h} = \dot{\theta} = 0$ one achieve:

$$
L \approx L_0 + \frac{1}{2}\rho c W_0^2 C_L'(\alpha)\left[\theta - \frac{\dot{h}}{W_0} - \left(\frac{1}{2} - a_{AC}\right)\frac{c\dot{\theta}}{W_0}\right] \qquad [N]
\tag{3.15}
$$

where the lift coefficient and its derivative $C_L' = dC_L/d\alpha$ are evaluated at $\alpha_0 = 0$. For thin airfoils it can be assumed that $C_L' = 2\pi$. The steady state lift force, L_0

has little influence on the stability of the airfoil, and can be assumed zero. The equations of motion with linearised lift can thus be written as:

$$\mathbf{M}\ddot{\mathbf{x}} + \mathbf{C}\dot{\mathbf{x}} + \mathbf{K}\mathbf{x} = 0 \qquad [-] \tag{3.16}$$

where $\mathbf{x} = \{h/c, \theta\}^T$. The matrices $\mathbf{M}$, $\mathbf{C}$ and $\mathbf{K}$ are defined as:

$$\mathbf{M} = \begin{bmatrix} 1 & -a_{CG} \\ -a_{CG} & r_{CG}^2 + a_{CG}^2 \end{bmatrix}, \quad \mathbf{C} = \frac{c\kappa}{W_0} \begin{bmatrix} 1 & \frac{1}{2} - a_{CG} \\ a_{CG} & a_{AC}\left(\frac{1}{2} - a_{CG}\right) \end{bmatrix},$$

$$\mathbf{K} = \begin{bmatrix} \omega_f^2 & -\kappa \\ 0 & r_{CG}^2\omega_t^2 - \kappa a_{AC} \end{bmatrix} \tag{3.17}$$

where $\omega_f = \sqrt{k_t/m}$ and $\omega_t = \sqrt{k_t/(mc^2 r_{CG}^2)}$ are the natural frequencies for the flapwise and torsional modes respectively without inertial coupling ($a_{CG} = 0$), and $\kappa = \frac{\rho}{2m}W_0^2 C_L'$ is the aerodynamic stiffness.

The aerodynamic damping matrix, $\mathbf{C}$, contributes only to small dissipative aerodynamic forces, which is assumed not to have any qualitative influence on the mechanism of flutter instability. But it is very important when calculating the exact critical flutter limit. As only the qualitative influences are studied here, it is possible to neglect the aerodynamic damping matrix, $\mathbf{C}$ to simplify the calculation. This lead to the following eigenvalue problem in equation 3.18, with $\mathbf{x} = \mathbf{v}e^{\lambda t}$, where λ is the eigenvalue and $\mathbf{v}$ is the eigenvector.

$$(\lambda^2 \mathbf{M} + \mathbf{K})\mathbf{v} = \mathbf{0} \qquad [N/m] \tag{3.18}$$

From this the following characteristic equation can be derived:

$$r_{CG}^2\lambda^4 + [(r_{CG}^2 + a_{CG}^2)\omega_f^2 + r_{CG}^2\omega_t^2 - \kappa(a_{AC} + a_{CG})]\lambda^2 + \omega_f^2(r_{CG}^2\omega_t^2 - \kappa a_{AC}) = 0 \qquad [1/s^2] \tag{3.19}$$

The eigenvalues are generally complex $\lambda = \beta + i\omega$. If the real part of one eigenvalue is positive, $\beta > 0$, then the equilibrium of the section is unstable. Using the Routh-Hurwitz stability criteria, the section is stable if

$$(r_{CG}^2 + a_{CG}^2)\omega_f^2 + r_{CG}^2\omega_t^2 - \kappa(a_{AC} + a_{CG}) > 0 \qquad [1/s^2] \tag{3.20a}$$

and

$$r_{CG}^2\omega_t^2 - \kappa a_{AC} > 0 \qquad [1/s^2] \tag{3.20b}$$

Using the first of these two limits (equation 3.20a) it can be found that the imaginary part is non-zero when the real part of the eigenvalue is positive, which leads to

oscillations. This limit can thus be used to define the critical flutter limit. Flutter occurs when the following inequality is true:

$$\frac{\rho}{2m}W_0^2 C_L' > \omega_f^2 \frac{r_{CG}^2 + a_{CG}^2}{a_{AC} + a_{CG}} + \omega_t^2 \frac{r_{CG}^2}{a_{AC} + a_{CG}} \quad \text{for} \quad a_{AC} + a_{CG} > 0 \qquad [1/s^2] \text{ (3.21)}$$

The flutter limit in equation 3.21, confirms the criteria in section 2.2. The flutter may occur under attached flow conditions, $C_L' > 0$, if the air-blade mass ratio, ρ/m and the relative wind speed, W_0 is sufficiently high for the aerodynamic forces to overcome the dynamic elastic forces represented by the uncoupled natural frequencies, ω_f and ω_t. These frequencies are weighted by some factors, and converge to infinity if the centre of gravity lies at the centre of mass ($a_{AC} + a_{CG} = 0$). If the centre of gravity lies in front of the aerodynamic centre, the inequality is never fulfilled for $C_L' > 0$. This is the reason why flutter can be avoided by putting weight at the leading edge on aircraft wings.

Using full stability analysis it was confirmed that the critical flutter speed decreases when the centre of gravity is moved further aft on the blade and decreases with lower uncoupled torsional frequency [2]. This is shown graphically in figure 3.6. QS mean that a quasi-steady approach is used. The other curves are made using unsteady aerodynamics. When comparing the full stability analysis and the single blade analysis the results for the critical flutter speed are similar. The work on classical flutter is still limited and no experimental data for modern commercial wind turbines are available for validation of the flutter limits.
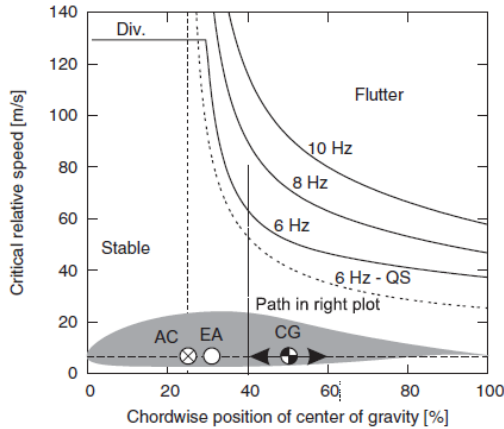
Figure 3.6: Flutter speed limits for a wind turbine section. The frequencies denote the torsional frequency. Modified from [2]

3.5 Stability analysis on wind turbines

To find out if a wind turbine is prone to flutter, an aeroelastic stability analysis has to be performed for the entire wind turbine structure. The tool which is used in this thesis, is the program HAWCStab2, created at Risø by M.H. Hansen [17]. This tool is buildt on the tool HAWCStab [3]. The basic principles of HAWCStab and HAWCStab2 are presented in this section.

3.5.1 Multi-blade coordinates

To be able to perform a stability analysis for the entire turbine, a multi-blade transform has to be performed. It describes the blade coordinates and deflections in a ground fixed frame of reference. As a result it eliminates the periodic coefficient from the equations of motion. Without this transformation it is very difficult to linearised and perform an eignvalue analysis of the wind turbine rotor.

The multi-blade transformations is also known as the Coleman transformation, and enables the individual blade coordinates to be described in the ground fixed frame of reference. The assumptions for using the multi-blade transformation are that the numbers of blades are odd, the inflow is uniform and the blades are identical and symmetrically mounted (isotropic rotor). Instead of a physical coordinate q_k for blade k, denoting flapwise, edgewise or torsional position, the multi-blade coordinates a_0, a_1 and b_1 are used. The multi-blade coordinates are defined through the transformation:

$$q_k(t) = a_0(t) + a_1(t)\cos\left(\Omega t + \frac{2\pi}{3}(k-1)\right) + b_1(t)\sin\left(\Omega t + \frac{2\pi}{3}(k-1)\right) \qquad (3.22)$$

$k = 1, 2, 3$ is the blade number. The letter a_0 describes the symmetric deflection of all blades. a_1 and b_1 are the asymmetric motions of the rotor. If the coordinate q_k describes the flapwise deflection of a blade, a_1 describes the tilt motion of the blade, b_1 the yaw motion of the blade and a_0 is the simultaneous flapwise deflection of the blades. If q_k describes edgewise deflection, a_1 and b_1 describe horizontal and vertical motions respectively and a_0 is the simultaneous edgewise deflection of the blades.

The multi-blade transformation enables the formulation of an eigenvalue problem. A solution of such a problem represent a mode of the turbine where the natural frequency ω is given by the eigenvalue, and the mode shape is given by the eigenvector in multi-blade coordinates, $a_0 = A_0 \sin(\omega t + \phi_0)$, $a_1 = A_a \sin(\omega t + \phi_a)$ and $b_1 = A_b \sin(\omega t + \phi_b)$. Substituted into equation 3.22 this leads to:

$$q_k(t) = A_0 \sin(\omega t + \phi) + A_{BW}\sin\left((\omega+\Omega)t + \frac{2\pi}{3}(k-1) + \phi_{BW}\right) + A_{FW}\sin\left((\omega-\Omega)t - \frac{2\pi}{3}(k-1) + \phi_{FW}\right)$$

$$(3.23)$$

The modal response of blade k may consist of three components: a symmetric component where all blades deflect simultaneously in the considered deflection shape with an amplitude A_0, and two cyclic components where the blades deflect with phase shift of $2\pi/3$ and the amplitudes A_{BW} and A_{FW} [2]. These modes represent the backward whirling and the forward whirling of the rotor. The blades vibrate in a forward or backward sequence relative to their numbering. The vibrations lead to the effective centre of mass of the rotor whirls about the rotor shaft, in the same or opposite direction of the angular velocity respectively. Most blade modes on a wind turbine is a combination of symmetric, forward whirling and backward whirling modes.

The frequency of the symmetric component is ω, while the frequency of the whirling modes are shifted by $\pm\Omega$. An observer on the blade would measure the frequency ω for all the modes, but as the multi-blade transformation transform the mode to a global point of view, the shift in the frequencies for the whirling modes is present.

3.5.2 Wind turbine structure

The wind turbine structure is defined with a multi-body formulation in HawcStab. Each part of the structure is defined as a substructure to the total structure, with its own relative coordinate system. Typical substructures are the tower, the shaft and the blades. The substructures are coupled with each other with algebraic constraints. Large rotations and translations are accounted for in the coupling points whereas small deflections are assumed within the objects [27]. The exception is the blade, where separate bodies within the blade are present. This type of formulation of the structure leads to a good management of large structural deflections. The different substructures are modelled with Timoshenko beam elements. The model of the wind turbine is illustrated in figure 3.7.

The Timoshenko beam theory includes the shear deformation and rotational inertia of the beam cross section. Each node thus has 6 DoFs: Two pairs of cross-sectional translations and rotations, a flapwise translation and a torsional rotation. The deformations on the turbine can be described with a node deformation vector $\mathbf{u} = \{\mathbf{u_t}, \mathbf{u_n}, \mathbf{u_{a_0}}, \mathbf{u_{a_1}}, \mathbf{u_{b_1}}\}^T$. $\mathbf{u_t}$ contains the tower substructure DoF, $\mathbf{u_n}$ contains the nacelle substructure DoFs described in the fixed frame of reference. $\mathbf{u_{a_0}}$, $\mathbf{u_{a_1}}$ and $\mathbf{u_{b_1}}$ describe the DoFs of the rotor blades in multi-blade coordinates.

In HAWCStab the steady state deformation of the turbine is assume dto be a steady state deformation of the rotot. In HAWCStab2, which is the version used in this thesie, the kinematics of the structure are based on a nonlinear co-rotational formulation. The element coordinate system $\mathbf{E_k}$ is continously updated according to the displacement of the nodes.

To find the equation of motion for the system, Lagrange's equation (equation 3.3) is applied on the structure. Then the results from Lagrange's equation is linearised,
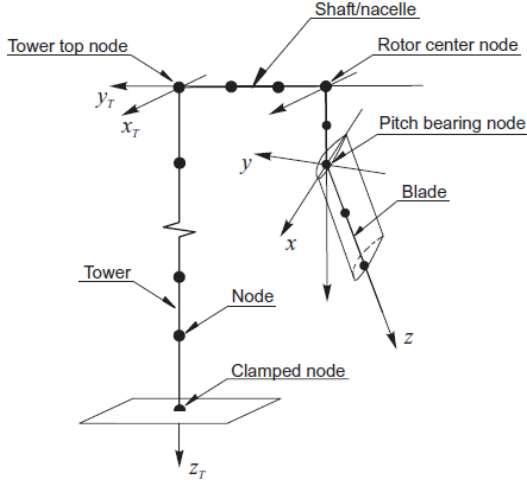
Figure 3.7: The beam element method used in HAWCStab

which leads to the linear equations of motion, found in equation 3.24. The different matrices in HAWCStab can be found in Hansen [3], and the different matrixes in HAWCStab2 can be found in Hansen [17].

$$\mathbf{M}\ddot{\mathbf{u}} + (\mathbf{C} + \mathbf{G})\dot{\mathbf{u}} + \mathbf{K}\mathbf{u} = \mathbf{Q} \qquad [N] \tag{3.24}$$

3.5.3 Coupling of the aerodynamics and the structure

The aerodynamic forces are assumed parabolic over the blade elements. To calculate the aerodynamic forces, the BEM method is combined with a Beddoes-Leishman type dynamic stall model. The aerodynamic states(equation 3.11) is combined with the BEM method, transformed to multi-blade coordinates and collected in an aerodynamic state vector: $\mathbf{z} = \{\mathbf{z_{a_0}}, \mathbf{z_{a_1}}, \mathbf{z_{b_1}}\}^T$. $\mathbf{z_{a_0}}$ contains the symmetric aerodynamic states, whereas $\mathbf{z_{a_1}}$ and $\mathbf{z_{b_1}}$ contains the asymmetric aerodynamic states.

The linear first order dynamic equation of the aerodynamic states can be written as:

$$\dot{\mathbf{z}} + \mathbf{A_d}\mathbf{z} = \mathbf{H}(\mathbf{u}, \dot{\mathbf{u}}) \qquad [1/s] \tag{3.25}$$

where $\mathbf{A_d}$ is a matrix having uncoupled 4x4 matrices in the diagonal, one for each aerodynamic calculation point. The vector $\mathbf{H}(\mathbf{u}, \dot{\mathbf{u}})$ is an inherent nonlinear function of the deformation vectors and velocity vectors. The function $\mathbf{H}(\mathbf{u}, \dot{\mathbf{u}})$

describes the effect of turbine vibrations on the angle of attack and relative inflow velocities at the calculation point. The matrixes can be found in [17], for HAWC-Stab2. In HAWCStab the equation is linearised about the symmetric deformations and the symmetric aerodynamic states as:

$$\mathbf{H}(\mathbf{u}, \dot{\mathbf{u}}) = \mathbf{C_{ux}}\dot{\mathbf{u}} + \mathbf{K_{ux}}\mathbf{u} \qquad [1/s] \qquad (3.26)$$

In HAWCStab2 the equation 3.25 is linearized about the steady state values of the aerodynamic states as found in [17].

3.5.4 Nonlinear steady state computation

In HAWCStab2 the equations are linearized about the nonlinear steady state. The nonlinear steady state is obtained for each operational point given by the wind speed, rotor sreed and pitch angle in an iterative process. First the steady state forces and moments in all aerodynamic calculation points are computed by BEM for the undeflected blade. Then the blade is deflected until there is an equilibrium of the external aerodynamic points computed by BEM and the moments with the internal elastic forces due to the element deformation. Then the aerodynamic forces are updated by a new BEM computation followed by a update of the blade deflection. This iterative proces continues untill the blade tip movement in an update is less than 0.01 % of the blade length.

3.5.5 Eigenvalue analysis

The aerodynamic and structural equations are linearized, and for each operational point the structural and aerodynamic coefficients are computed using Gauss integration of analytical funtions of the position vectors and rotation matrices and their derivatives. The linearised equations are then collected in the coupled aeroelastic equations which describes the blade response to small vibrations about the steady state equilibrium.

$$\mathbf{M}\ddot{\mathbf{u}} + (\mathbf{C} + \mathbf{G} + \mathbf{C_a})\dot{\mathbf{u}} + (\mathbf{K} + \mathbf{K_a})\mathbf{u} + \mathbf{A_f}\mathbf{z} = 0 \qquad [N]$$
$$\dot{\mathbf{z}} + \mathbf{A_d}\mathbf{z} + \mathbf{C_{uz}}\dot{\mathbf{u}} + \mathbf{K_{uz}}\mathbf{u} = 0 \qquad [1/s] \qquad (3.27)$$

To be able to study the natural frequencies and the damping of the wind turbine blades, an eigenvalue analysis is performed. It is possible to obtain a direct formulation of the eigenvalue problem from equation 3.27, but this method leads to an ill-conditioned problem. To avoid that, a modal expansion of the DoFs is performed. The undamped eigenvectors of the turbine at standstill, $\omega_\mathbf{i}$ is used for this expansion, where N is the number of natural modes, $\mathbf{\Phi}$ is the modal matrix containing the undamped eigenvectors, and $\mathbf{v}$ is the new structural state vector.

$$\mathbf{u} = \sum_{i=1}^{N} \omega_{\mathbf{i}} v_i(t) = \mathbf{\Phi v} \tag{3.28}$$

After the modal extension, the aeroelastic states are gathered in a vector $\mathbf{y} = \{\mathbf{z}, \mathbf{v}, \dot{\mathbf{v}}\}^{\mathbf{T}}$, and solutions to the eigenvalue problem on the form $\mathbf{y} = \mathbf{w} e^{\lambda t}$ is sought. Inserting this equation into equation 3.28 and the result into equation 3.27, one obtains the following eigenvalue problem:

$$\left(\begin{bmatrix} \mathbf{A_d} & \mathbf{K_{uz}\Phi} & \mathbf{C_{uz}\Phi} \\ \mathbf{0} & \mathbf{0} & \mathbf{-I} \\ \mathbf{\Phi^T A_f} & \mathbf{\Phi^T (K + K_a)\Phi} & \mathbf{\Phi^T (C + G + C_a)\Phi} \end{bmatrix} + \lambda \mathbf{I} \right) \mathbf{w} = \mathbf{0} \tag{3.29}$$

The eigenvalues, λ_n, and eigenvectors, w_n yield the natural frequencies, the damping and the mode shapes of the aeroelastic turbine modes. The natural frequency and logarithmic decrement for mode nr n are given by the imaginary and real parts of the eigenvalues respectively. Instabilities of the wind turbine can be found where the aeroelastic damping of a mode is negative.

$$f_n = \frac{\text{Im}\{\lambda_n\}}{2\pi} \qquad [Hz] \qquad \text{and} \qquad \delta = -\frac{\text{Re}\{\lambda_n\}}{f_k} \qquad [-] \tag{3.30}$$

3.5.6 Campbell diagram
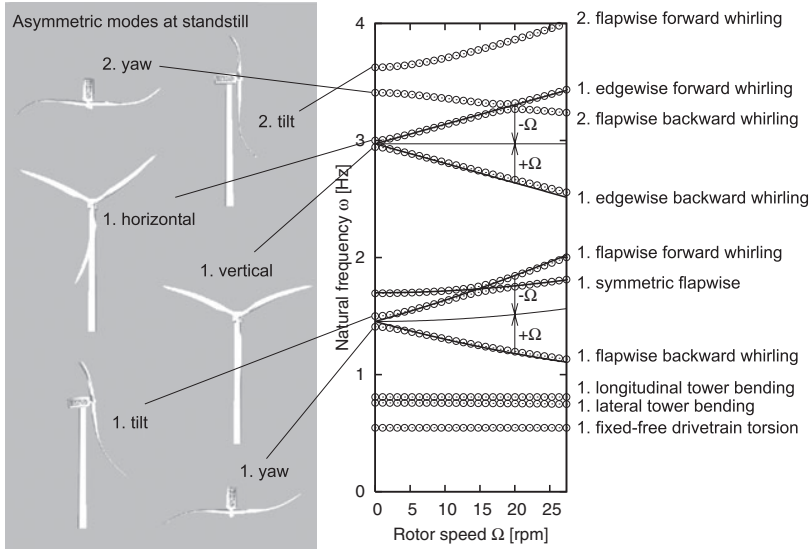
Figure 3.8: Exampel of Campbell diagram, from Hansen [2]

25

To understand how the modes vary with the rotational speed of the wind turbine and the effect of the multi-blade transformation, the Campbell diagram of a wind turbine is explained. Figure 3.8 shows the Campbell diagram for the lower order turbine modes. The natural frequency of the turbine modes are plotted against the rotational speed of the rotor. There are no aerodynamic forces on the blade, only the increasing rotational speed.

The modes with the lowest natural frequency are the low order tower modes: The 1. fore-aft bending mode and the 1. side-to-side bending mode. The natural frequency of the structural tower modes is practically independent of the rotational speed of the rotor. As the generator is a direct-drive generator, there is no mode present which represent the drive train torsion, instead there is a mode consisting of the symmetric edgewise bending of the modes [2].

The blade modes are described using multi-blade coordinates. There are thus one symmetric, one forward whirling and one backward whirling mode for each blade mode. The backward and the forward whirling modes have natural frequencies which shifts with $\pm\Omega$ and the rotational frequency Ω increases. This is due to the multi-blade transformation.

The symmetric blade modes are mainly constant as the relative wind speed increases. The 1. edgewise symmetric deflections is dependent on the torsion of the shaft and the operation of the generator, and thus the natural frequency of the 1. edgewise symmetric mode is mainly independent of the rotational speed. The 1. symmetric flapwise mode has a frequency which increases due to centrifugal stiffening as the rotational speed increases. This effect is also present in the flapwise forward and backward whirling modes. Centrifugal stiffening is the effect of the centrifugal force on the blade stiffness. The centrifugal forces try to force the blades into a position which is as close as possible to perpendicular to the shaft. As a result the stiffness of the blade increase and the frequency of the vibrations increase.

The blade stiffness is higher in the edgewise direction than in the flapwise direction. The 1. edgewise mode has thus a higher frequency than the first edgewise mode

3.5.7   Other methods for stability anlayses

The method used in HAWCStab2 is not the only method to be used for stability analysis. In different studies different approaches are used to finding the critical flutter speed. A short description of the method used in some of these studies are described here.

A aeroelastic stability tool which models the whole wind turbine is developed by Riziotis and described in [19]. The structure of the wind turbine is approximated with beams bending in two directions, flapwise and torsion. The Lagrange equation (3.3) is used to derive the equations of motion. The aerodynamic forces are modelled using BEM and the ONERA Lift and Drag dynamic stall model. The

multi-blade transformation is performed and the coupled equation of motion is linearised to be able to perform an eigenvalue analysis.

An aeroelastic stability predictions for a MW-sized blade was performed by Lobitz [8]. Only a single blade was simulated and not the entire turbine. The calculations are similar to the derivation in section 3.4, but focuses on the whole blade, and does not apply the simplifying assumptions. The focus of the unsteady aerodynamic effects is the shed wake, and a version of Theodorsn's theory modified for wind turbines is used as aerodynamic model. The blades are modelled using a NASTRAN tapered beam element. The equation of motion was found, linearised, and used in the eigenvalue analysis.

A low-order model for blade analysis, which also has the possibility to model flutter was described by Kallesøe. This applied the Beddoes-Leishman type dynamic stall model for the unsteady aerodynamics and Lagrange equation to derive the structural model.

3.6 Time domain analysis

To study the response of a wind turbine in different conditions, a time domain analysis can be performed. The time-domain analysis is a standard tool to find the response of a wind turbine. It is possible to observe the effect of flutter in time domain simulations. The flutter vibrations are mainly vibrations in the flapwise and torsional direction with rapidly increasing amplitude at high relative wind speeds, and can thus be recognized. The flutter vibrations appear in the attached flow regime at high relative velocities. An advantage of the time-domain simulations compared to an eigenvalue analysis is that more non-linearities can be express as the equations of motions need not be linearised.

In this thesis the aeroelastic simulation tool HAWC2, developed at Risø DTU [28] is used to study the effect of aeroelastic instabilities in the time domain.

3.6.1 The aeroelastic simulation tool HAWC2

The aeroelastic stability tool HAWCStab2 is developed from HAWC2, so the main principles of the tools are mainly the same, except for the linearization and eigenvalue approach in HAWCStab2. The wind turbine structure is defined with a multi-body formulation, where the substructures are coupled with algebraic constraints.

The aerodynamic in HAWC2 is described using the Blade Element Momentum (BEM) method. The induced velocities in BEM are defined locally on a non-rotating polar grid, which enables the possibility for different induction in top and bottom of the rotor. To account for the aerodynamic tip-loss on the blades, Prandtl's tip-loss method is used. This method is explained in Manwell [25]. To

calculate the dynamic stall Øyes method or the Beddoes-Leishman method can be chosen. The Beddoes-Leishman method is discussed in section 3.3 and Øyes method is a simplified version of the Beddoes-Leishman method. Aerodynamic drag on the different substructures is implemented together with tower shadow effects. The wind can be described using both turbulence and wind shear from the atmospheric boundary layer. It is also possible to implement wakes from other wind turbines and floating wind turbine structures in HAWC2.

Chapter 4

The Reference Turbine

The wind turbine studied in this thesis is designed by Lars Frøyd [4]. The design of this wind turbine is a part of a project by NOWITEC, Norwegian Research Centre of Offshore Wind Technology, to design a reference turbine. The turbine is still in the design process, which this thesis is a part of. A summary of the turbine design parameters is found in table 4.1:

Rotor configuration	3-bladed, upwind, pitch control
Rated power	10 MW
Cut-in wind speed	5 m/s
Cut-out wind speed	25 m/s
Design wind speed	13.25 m/s
Rotor diameter	140.4 m
Maximum allowed tip speed	90 m/s
Design tip-speed ratio (TSR)	7.3
Electromechanical efficiency	92 %
Tower height	110 m
Generator configuration	Direct drive variable speed generator

Table 4.1: Wind turbine specifications

4.1 The blades

The diameter of the rotor is 140 m and each blade is 69 m and is made of composite material. The wind turbine is designed to have 3 blades which are identical. The diameter of the rotor is determined by the design wind speed, which is the wind speed where the turbine reaches rated power. Longer blades result in a wind turbine which captures more energy of the wind and thus reaches rated power at a lower wind speed. Different types of airfoils are used along the blade span to achieve a

high energy production. The airfoils and chard thickness along the blade span is shown in figure 4.1.
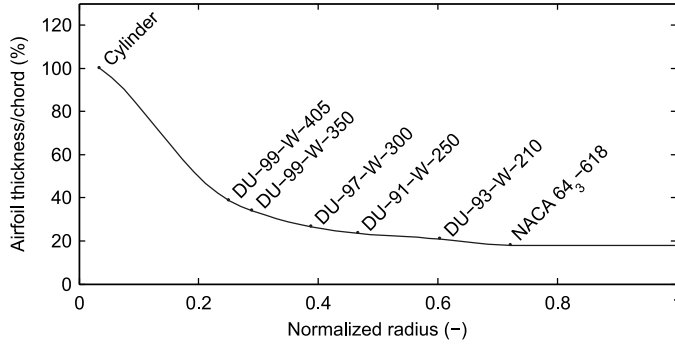
Figure 4.1: Airfoil thickness and profile distribution, from Frøyd [4]

The chord length and twist of the blades is optimised using the Blade Element Momentum (BEM) method, using the method described by Frøyd [29].

The internal structure of the blades is indicated in figure 4.2. The blade consists of a skin made of composite material, mainly fibreglass and foam. Inside the skin there is a central beam, called a spar cap, built up of thicker laminated material including fibreglass and carbon fibres. The upper and lower spar caps are held together by shear webs which run along the length of the spar. The airfoil-shaped skin and the spar cap are the main load carrying components. The shear webs are designed to distribute the shear forces between the spar caps and contribute to the edgewise and flapwise stiffness of the blade.
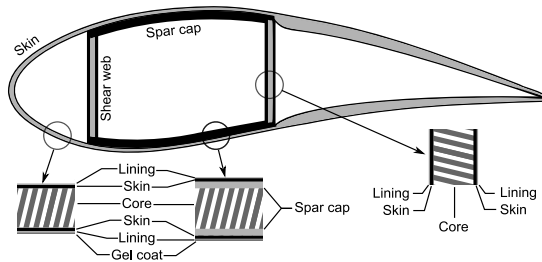
Figure 4.2: Cross section and composite layout. From Frøyd [4]

The hub is simulated in this thesis as 3 uniform cylinders, which have the blades attached to the end, instead of a real hub configuration. This is to simplify the input data to the aeroelastic tools. The hub length is set to be 2,5 m and the hub
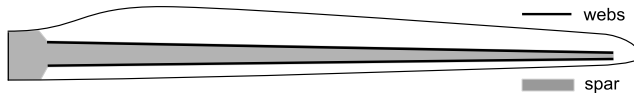
Figure 4.3: Layout of the spar and shear webs. From Frøyd [4]

mass is 75 ton. The nacelle and shaft structure is 5 m long. The total mass at the top of the tower is set to be 400 ton.

In the aeroelastic analysis in this thesis, 3 different blades are studied, one baseline one stiff and one soft blade. The shape of the blades is the exact same, the only difference between them are the stiffness. The stiffness of the blades in the different directions are found in figure 4.4

The baseline blade is the blade which is planned to be used on the reference turbine. More information on the design of this blade can be found in Frøyd [4]. The blade parameters of this blade is found in appendix C.1. The soft blade is approximately 20 % softer than the baseline blade in all directions. The stiff blade has approximately the same stiffness as the baseline blade in flapwise and edgewise direction. In torsional direction it is approximately 50 % stiffer than the baseline blade.

The hub of the blades is simulated in this thesis as 3 uniform cylinders, which have the blades attached to the end, instead of a real hub configuration. This is to simplify the input data to the aeroelastic tools. The hub length is set to be 2,5 m and the hub mass is 75 ton. The nacelle and shaft structure is 5 m long. The total mass at the top of the tower is set to be 400 ton.

4.2   Tower and support structure

The tower of the wind turbine is tubular and is made of steel. The height of the tower is 110 m. The tower stiffness is chosen to be soft-stiff, which means it has a natural frequency between 1P and 3P. 1P is the rotational frequency of a blade and 3P is the blade passing frequency for a 3-bladed wind turbine.

The turbine is planned to be a floating offshore turbine. The floating platform is planned to be a Tension Leg Platform. The intention is to use a four-legged lattice substructure for the 10 MW wind turbine, possibly integrating the tower and the foundation in one piece. But for preliminary analysis like in this thesis, a standard tubular tower is used, and the tower is assumed to be bottom-fixed.

(a) Flapwise stiffness

(b) Edgewise stiffness

(c) Torsional stiffness
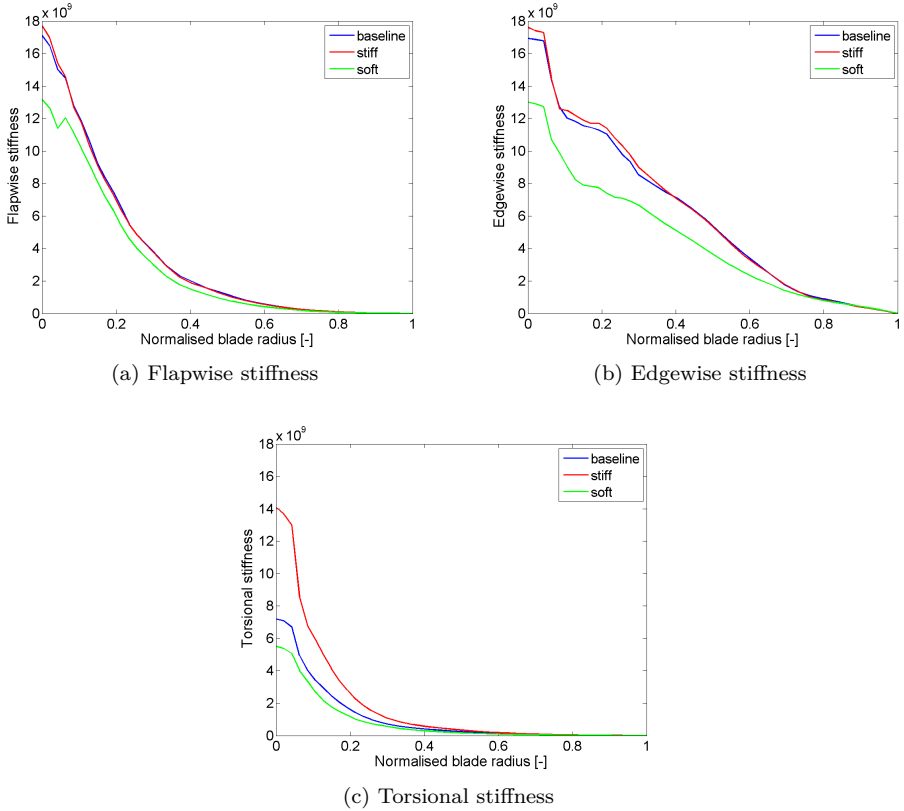
Figure 4.4: Stiffness in different directions

4.3 Drive train and control system design

The wind turbine is designed to operate at variable speed and variable pitch. The concept chosen to achieve this is a direct drive permanent magnet synchronous generator with a fully rated converter [4]. It is chosen as a compromise between weight, reliability and the ability to meet grid code requirements.

The main goal for the control system is to minimize the costs during the lifetime of the turbine. The energy capture should be as high as possible for every wind condition without surpassing neither the rated power nor the maximum blade tip speed. An ideal power curve, with regions of different control objectives is shown in figure 4.5. Region 1 has wind speeds below the cut-in speed and the turbine is not operating. In region 2 the wind speed is above cut-in and below rated and the turbine should be operated at maximum efficiency to extract the maximum available power from the wind. In region 3, above the rated wind speed, the blades must be pitched, to avoid that the power output become higher than the rated

power and the forces on the structures too high. In region 4 the wind speed is above the cut-out speed, and the wind turbine is shut down to avoid damage. To achieve this, the blades are pitched to feather. The highest thrust and highest forces appears in the transition region 2 1/2, when the turbine reaches maximum rotational speed, but before the blades begin to pitch.
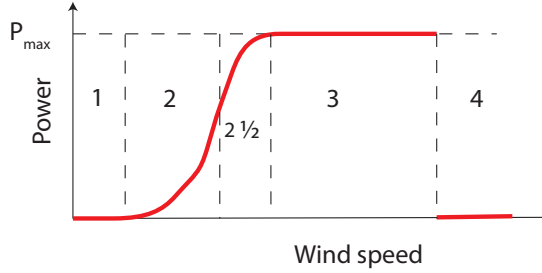
Figure 4.5: Ideal power curve

Some control parameters can be found in figure 4.6, which shows the operation of the control system. The TSR and the pitch angle is kept constant in region 2, to achieve as high as possible power coefficient, until the rotational velocity Ω reaches its maximum value. This value is set to avoid too high tip speed of the blades. In region 2 1/2, Ω is kept constant and TSR drops according to equation 4.1. When the rated power is reached, the blades are pitched to keep the power constant.

$$TSR = \frac{\Omega R}{V} \tag{4.1}$$
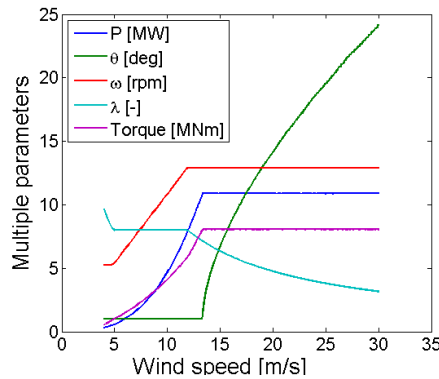
Figure 4.6: Controlled parameters for the baseline case

33

Chapter 5

Methodology and Validation

5.1 Aeroelastic stability analysis

In this thesis the wind turbine presented in chapter 4 is analysed, to study if it is prone to flutter. The study is performed using the aeroelastic stability tool HAWC-Stab2. The theory behind this tool is discussed in chapter 3.5. HAWCStab2 runs an eigenvalue analysis of the turbine. The results show the aeroelastic frequencies and the damping of the turbine modes. If a mode shape has negative damping, it indicates an instability of the wind turbine.

The turbine modes are computed at different operating points. The operating points are defined by the rotational speed of the turbine, the wind speed and the blade pitch. In this study the goal is to investigate aeroelastic instabilities and the critical flutter limit. As the flutter limit is dependent on the relative wind speed on the blade, it is convenient to set the operating points such that it reflects this. As the program computes the aeroelastic frequency and damping versus the incoming wind speed, the operating points where chosen such that the relative wind speed at the blade tip is 10 times the wind speed. This is achieved by using a tip-speed ratio (TSR) of $\sqrt{99}$ when calculating the rotational speeds, using equation 4.1. The operational points which were used is found in table 5.1. In the analysis both the relative wind speed and the incoming wind speed increases. The highest operating speed in the simulations was chosen to be a relative wind speed of 220 m/s. The blade pitch is set to zero for all wind speeds.

Wind speed [m/s]	Pitch [deg]	Rotational speed [rpm]
2.0	0.0	2.7
5.0	0.0	6.7
8.0	0.0	10.8
10.0	0.0	13.5
12.0	0.0	16.2
14.0	0.0	18.9
16.0	0.0	21.6
17.0	0.0	22.9
18.0	0.0	24.3
19.0	0.0	25.6
20.0	0.0	26.9
21.0	0.0	28.3
22.0	0.0	29.7

Table 5.1: Operational points for analysis in HAWCStab2

Simulations of the wind turbine in normal power producing operation were also performed, to study if the wind turbine experienced instabilities in normal operation. To find the operating points, a control system was applied. The operating points were chosen using this control system to find the rotational speed and the blade pitch at the different wind speeds. The operational points used for all the different blades are found in table 5.2. The control system strategy is discussed in chapter 4.3.

Wind speed [m/s]	Pitch [deg]	Rotational speed [rpm]
3.0	1.72	5.5
5.0	-0.29	5.5
6.0	-0.43	6.2
8.0	-0.45	8.2
10.0	-0.45	10.3
12.0	-0.45	12.2
13.0	-0.45	12.2
14.0	3.46	12.2
16.0	8.07	12.2
18.0	11.18	12.2
21.0	14.97	12.2
25.0	19.24	12.2

Table 5.2: Operational points for normal power production

In the analysis of the baseline blade, one analysis was performed where the steady state downwind deflection of the blade was neglected. This was done to study the effects of the deflection of the blade. A analysis of the turbine in HAWCStab2,

without deflection of the blades correspond to the use of the aeroelastic stability tool HAWCStab.

When setting up the input files to the stability simulation, the turbine is modelled to have a free rotation constraint between the tower and the shaft. This is because the instabilities are found at such high rotational speed, that the turbine in reality would have to be cut off from the grid, else it would burn up. This assumption is important because the simultaneous edgewise mode is dependent on the torsion of the shaft and thus on the moment of the generator. An example of the input file to HAWCStab2 and the file with the operating points is found in appendix C.

It is possible to run the aeroelastic stability analysis as an isolated blade simulation or as an entire turbine simulation. The isolated blade simulation simulates only one blade, and does not account for the effects of the tower and shaft on the vibrations. In the entire turbine simulations these effects are included. Both of these methods are used in this study.

The program used in this simulation, HAWCStab2 is a new tool. There has not yet been published any papers of the entire tool, only on the blades [17]. During the work of this thesis, several updates was made on this tool, and currently version 97 is used. The results from this thesis are also used to debug the tool. Some days before this thesis was finished there were found some bugs in version 97, and a new version of this tool was constructed. These bugs and how it affects the results are discussed in appendix B.

5.1.1 Aeroelastic frequency and damping

The results from HAWCStab2 describes the aeroelastic frequency and damping of the different modes. The aeroelastic frequency describes the vibrations of the blades due to the elasticity of the blades and the influence of the wind speed and the rotational speed. The wind speed and the rotational speed excite the blade to vibrate with different deflection modes. As the wind speed increases, different modes may couple with each other. An example of this is torsion of the blade due to to the misalignment of the centre of gravity and the centre of lift as the blades deflect downwind due to high wind speed. A mode at high wind speed may be a combination of flapwise and edgewise motion, blade torsion and tower motion.

The damping of the aeroelastic modes describes how much the amplitude of the vibration decreases after an initial excitement. The damping is measured as the logarithmic decrement of the vibration, which is defined in equation 5.1

$$\delta = ln\frac{x(t)}{x(t+\tau_d)} = \frac{2\pi\xi}{\sqrt{1-\xi^2}} \qquad [-] \qquad (5.1)$$

δ is the logarithmic decrement, $x(t)$ is the amplitude at time t and $x(t+\tau_d)$ is the amplitude at time $t+\tau_d$. ξ is the damping coefficient of the system. If a mode has

a high logarithmic decrement, the vibrations of this mode are soon damped out. If the damping is low, the vibrations use long time to dampen out. If the aeroelastic damping is negative it implies that the vibrations have increasing amplitude, and that the system is unstable. The damping of the blades is dependent on the rotational speed and the wind speed.

5.2 Simulations in the time domain

To study the response of the wind turbine to aeroelastic instabilities, simulations in the time domain was performed, using the aeroelastic simulation tool HAWC2. To make the result comparable to the aeroelastic stability analysis, uniform incoming wind was used. One simulation was run with wind shear, tower shadow and turbulent wind, to study how the realistic wind conditions would influence the triggering of aeroelastic instabilities.

Simulations of how the turbine behaves when the connections to the power grid is lost was performed. This is known as run-away condition. To achieve this in the simulations, a free bearing between the shaft and the tower was used, such that the rotor could rotate freely. The wind speed was set to 10 m/s and the rotational speed was set to have an initial velocity of 10.4 rpm.

A simulation was performed with increasing wind speeds and constant rotational speeds. This was done for several rotational speeds. The generator was set to be working and controlling the rotational speed. In each simulation the rotational speed was kept constant and the wind speed was set to increment 1 m/s every 50 seconds. The wind speed varied from 5 m/s to 20 m/s. This simulation was performed for rotational speeds from 10 rpm to 26 rpm. The simulation was performed to get a better picture of when and why the instability appears.

5.3 Validation

To validate the simulations, they should be compared against experiments. As no experiments have been performed on wind turbines this size, this is not possible. Instead a code to code comparison was performed. There are no other comparable aeroelastic stability codes available, which HAWCStab2 could be validated against. But the input to HAWCStab2 is mainly the same as the input to HAWC2. There exists aeroelastic stability tools which are comparable to HAWC2, and thus HAWC2 was used for validation. To validate the input to the aeroelastic simulation program HAWC2, the results from HAWC2 was compared with simulation result from the Blade Element Momentum (BEM) method, and the results from the aeroelastic simulation tool FAST.

The BEM method is a method to calculate the aerodynamic properties of the wind turbine blades. It is simplified and not considering unsteady aerodynamic effects.

The BEM method is described shortly in chapter 3.3, and more thoroughly in Manwell [25]. Both FAST and HAWC2 uses BEM to calculate the aerodynamic forces on the blades. In FAST and HAWC2, unsteady aerodynamic effects are also considered. The version of BEM used in this validation is created by Lars Frøyd.

FAST is a aeroelastic simulation tool made by NREL, the National Renewable Energy Laboratorium in the United States. The purpose of FAST and the manner of operation is similar to HAWC2, but the details in the calculations are different. HAWC2 uses beam element theory to calculate the deflection of the beam element, whereas FAST uses a modal approach. In FAST it is assumed that the deflection of an element is a linear combination of the modal shapes of the element. More information on FAST is found in the FAST user guide [14]. There are two different ways to calculate the response in FAST: One steady calculation which uses the equilibrium inflow model and one dynamic calculation which uses the generalized dynamic wake model. In this validation the dynamic model is used, as the FAST user guide [14] states that this model should be used for production runs.

The inputs to the programs are different, but the wind turbine it describes should be the same. The stiff blade was simulated. There may be some differences in the turbine which is simulated due to the different methods used for defining the wind turbine structure the input files. There is assumed to be no tilt and cone angles. The simulations were performed with uniform incoming wind at 10 m/s and a rotational speed of 10 rpm.

5.3.1 Result from code to code comparison

	HAWC2	FAST	BEM
Power [MW]	4802	4799	4679
Cp	0.502	0.502	0.489
Thrust [kN]	791	791	735
Blade flapwise moment [kNm]	10 060	10 690	11 313
Blade displacement [m]	4.6	4.2	-

Table 5.3: Comparisment different codes at 10 m/s and 10.4 rpm, averaged values

	HAWC2	FAST	BEM
Power	0	-0.1 %	-2.6 %
Cp	0	-0.1 %	-2.6 %
Thrust	0	0.0 %	-7.0 %
Blade flapwise moment	0	6.3 %	12.5 %
Blade displacement	0	-8.9 %	-

Table 5.4: HAWC2 compared to the other codes. Percentage difference from HAWC2 results

In table 5.3 and table 5.4 the results from the code to code comparison is found. The BEM method has not blade deflection implemented, and no blade displacement is found in the BEM method. In FAST the torsional bending of the blades is not implemented.

As seen in the tables, the HAWC2 code gives higher values than the other codes, except for the blade flapwise moment. The results from the dynamic simulation in FAST are approximately the same as the values in HAWC2, with 0 % difference at the best, when ignoring the blade flapwise moment and the blade deflection. The results from BEM are between 2 % and 7 % lower than the results from HAWC2. The high flapwise moment from BEM may be the result of a blade which does not deflect downwind. A deflection of the blade downwind leads to centrifugal forces acting on the blade, reducing the blade root moment. It is curious though that the rotor thrust of the BEM method is the lowest of the three codes, but the flapwise moment is the lowest. When using another code, WT_Perf, to calculate BEM, the results was the same, except for a higher rotor thrust in WT_Perf. The thrust for the BEM is thus not certain to be correct. No obvious reason is found for the high blade moment in FAST or a low blade moment in HAWC2.

In the IAE Offshore Code Comparison Collaborative (OC3) [30] different aeroelastic codes were compared to each other. The power output from FAST was found there to be approximate 5 % higher than the power output from HAWC2. The blade simulated was another blade, and the results are thus not directly comparable. In this validation study the results from HAWC2 and FAST is found to be very similar. The results from BEM were found to be slightly lower than the results from BEM and HAWC2. This may be due to the fact that BEM is a simplified method, not accounting for the linearities and dynamic which is implemented in FAST and HAWC. The slight difference between HAWC2 and FAST may be due to the torsional degree of freedom which is not implemented in FAST. Some differences between the codes may be due to the different design of the codes, using different input files and different computational schemes. When using the steady calculations in FAST, the results are found to be between 4 % and 8 % lower than the results from HAWC2 and the dynamic simulation in FAST. This shows that a difference in the calculation my result in differences between the results of the codes. As the results from HAWC2 and FAST are so similar, the input to HAWC2 can be said to be validated. Due to this it is assumed that the input to the aeroelastic stability analysis is correct.

Chapter 6

Results and Evaluation

The most important results are presented in this section. Some discussion of the results is also found in this section, together with the plot of the results. An overview of the results and a more general discussion with comparison to other studies is found in chapter 7. For the aeroelastic stability analysis in this thesis, version 97 of the aeroelastic stability tool HAWCStab2 is used.

6.1 Baseline blade

The baseline blade is the blade which is planned to be used on the NOWITECH reference turbine. The blade is analysed to find the critical flutter speed and if it is prone to flutter in normal operation. The turbine is also simulated in the time domain using the aeroelastic tool HAWC2. The results from the time domain show how the wind turbine reacts to flutter instabilities. The flutter limits found in the different analyses are then compared with each other.

6.1.1 Aeroelastic stability analysis

Aeroelastic stability analyses were performed to study what creates aeroelastic instability and at which wind speeds and frequencies the instabilities occurs. Aeroelastic eigenvalue analysis can reveal information that no simulations in the time domain can reveal, but it does not show the actual movements and response of the wind turbine. The analysis assumes uniform and steady incoming wind.

In the results from HAWCStab2, the different modes at each operational point are not sorted. Deciding which mode belongs to a mode in the previous operational point and sorting them are done manually. This is a source of error, especially when discussing which mode becomes negative. Smooth lines between the operational

points in the frequency and in the damping plots are considered together with the animation of the mode shapes.
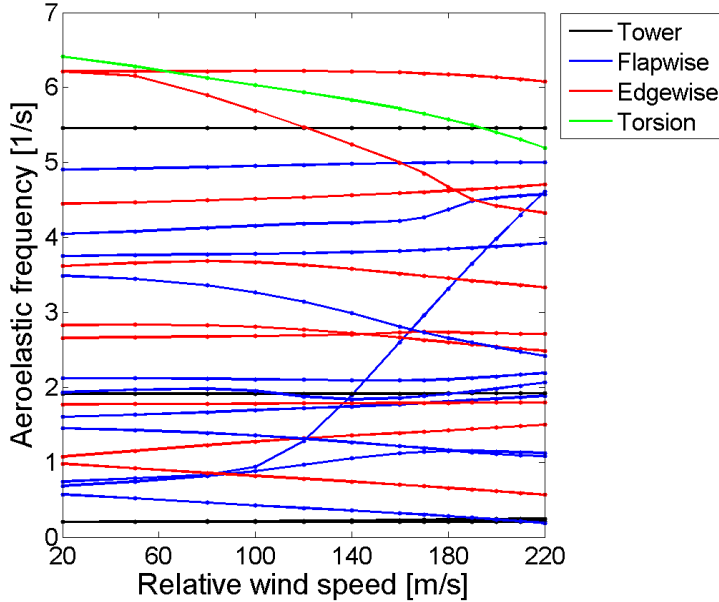
Figure 6.1: Aeroelastic frequency plot for the entire turbine analysis with baseline blades

The aeroelastic frequency of the 20 first modes for the baseline blade can be found in figure 6.1. As the rotational speed increases the forward and backward whirling modes are shifted $\pm\Omega$, due to the definition of whirling modes as discussed in chapter 3.5.6. In addition to this, effects of the wind on the blades are present.

One of the modes which have a significant increase in the aeroelastic frequency as the relative wind speed increases is the first symmetric flapwise mode. The phenomena which leads to this is known as aeroelastic stiffening, and is due to the coupling of the first torsional flapwise symmetric mode with torsion. As the profile accelerates up to a higher velocity, the blade pitches nose-up due to the aft centre of mass on the blade. This leads to a higher angle of attack on the blade and thus higher lift forces in the direction of the acceleration. The aerodynamic forces are out of phase with the deflection of the blade, which leads to increased stiffness of the blade.

The decrease in the frequency of the 1. torsional mode is due to the aft centre of mass on the turbine. The effect can be found in equation 3.17 in the part of the stiffness matrix which describe the torsional stiffness: $r_{CG}^2\omega_t^2 - \kappa a_{AC}$. As the relative wind speed increases, κ increases proportionally, leading to a reduced torsional stiffness at increased relative wind speeds.

It is possible to run aeroelastic stability analyses with unsteady aerodynamics or quasi-steady aerodynamics. An analysis performed with quasi-steady aerodynamics showed that the wind turbine becomes unstable at lower relative wind speed with quasi-steady aerodynamics, than with unsteady aerodynamics. This confirmed Lobitz [8] theory that quasi steady results are very conservative. To be able to include the unsteady aerodynamic effects in this study, unsteady aerodynamics was used.

6.1.2 Modes which cause instability

To study if and when the blade becomes unstable, the modes with negative aeroelastic damping are studied. The turbine is analysed as an isolated blade and as an entire turbine.

Isolated blade

(a) Frequency
(b) Damping
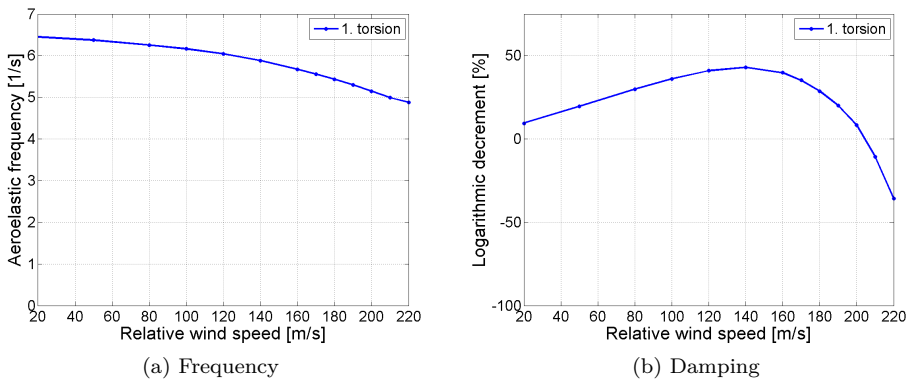
Figure 6.2: Modes which cause instability in the isolated blade analysis with baseline blades

When the results from the aeroelastic stability analysis of an isolated blade are studied, only one mode is found to have negative damping. This mode is shown in figure 6.2. The mode which has negative damping is the 1. torsional mode. At low relative wind speeds the mode consists mainly of torsional motions, but as the wind speed increases, the torsional motion couples with flapwise motion. The torsional motion leads to changes in the angle of attack, which causes changes in the aerodynamic forces and leads to flapwise vibrations. The aeroelastic frequency of the mode decreases as the wind speed increases and it couples with flapwise motion. When the mode becomes unstable, the aeroelastic frequency is 5 Hz. As the torsional mode couples with the flapwise motion, the aerodynamic forces begin to act in an unfavourable phase with the flapwise deflection of the blade, and a

flutter mode is created. The mode has flutter-like motion and the typical steep decrease in aeroelastic damping.

Entire turbine

(a) Frequency   (b) Damping
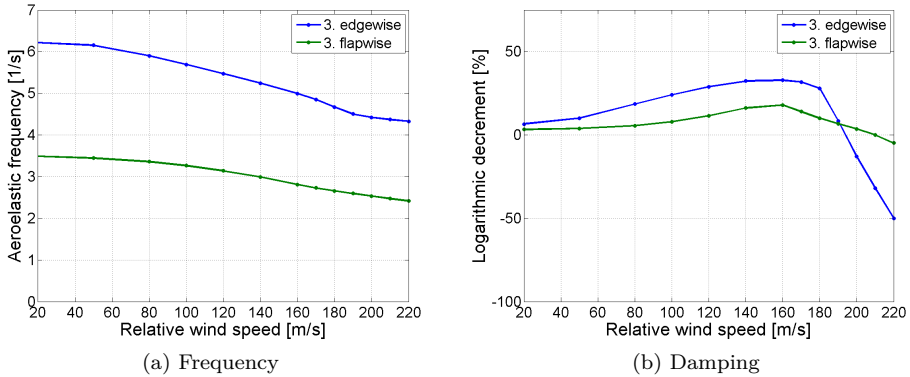
Figure 6.3: Modes which cause instability in the entire turbine analysis with baseline blades

In the entire turbine analysis, two modes were found to have negative damping. These modes are found in figure 6.3.

The first mode with negative damping is the 3. edgewise symmetric mode. It becomes negative damped at a relative wind speed of 200 m/s. At low relative wind speed this mode is edgewise but slightly coupled with torsional motion. As the relative wind speed increases the mode couples with torsion, and at high relative wind speeds, the mode couples with flapwise motion and becomes a flutter mode. The mode has a frequency of 4.4 Hz as it becomes unstable. The motions of the mode are a combination of flapwise and torsional motion, and the damping has the typical steep negative damping of flutter. This indicates that this mode becomes the flutter mode.

It is a question why the 3. edgewise mode becomes unstable and not the 1. torsional mode as in the analysis of the isolated blade. The difference between the entire turbine analysis and the isolated blade analysis is that the effect of the shaft and the tower motions are present in the entire turbine analysis. In addition the effects of all the blades are present in the entire turbine simulation, and the blade modes are expressed in multi-blade coordinates. In other studies of flutter instabilities, torsional or flapwise modes become unstable with flutter motion. This is expected as the flutter mode consists of torsional and flapwise motion. In the plot of all the aeroelastic frequencies in figure 6.1 it can be found that the frequency of the 3. edgewise symmetric mode is very close to the frequency of the 1. torsional

backward whirling mode at low wind speeds. Even at zero wind speed, the modes couple due to the close frequency and at around 800 m/s the mode is almost purely torsional. This coupling is probably due to the close frequency of the modes and the geometrical coupling between edgewise motion and torsion due to the steady state deflection of the blade. The animations of the 1. torsional mode in the isolated blade analysis is similar to the animations of the 3. edgewise symmetric mode in the entire turbine analysis, even at quite low wind speeds. The mode is entirely torsional before it couples with the flapwise mode into the flutter mode. A possible reason for the 3. edgewise mode becoming the flutter mode, may be that as the frequency of the 3. edgewise symmetric mode decreases more than the 1. torsional backward whirling mode, it may couple easier to the flapwise mode to create flutter. At high relative wind speed the aeroelastic damping of the 1 torsional backward whirling mode decreases, and it is possible that this mode becomes negative damped at a higher relative wind speed. A visualisation of the blade flutter mode is found in figure 6.4
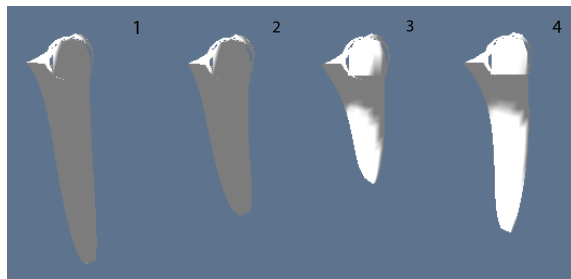
Figure 6.4: Blade flutter mode

The next mode which has negative damping is the 3. flapwise mode. It becomes unstable at a relative wind speed of 210 m/s and with a frequency of 2.5 Hz. The animation of this mode shows the typical flutter-like motion, but with moderate levels of negative damping. The moderate levels of negative damping may indicate that only some of the airfoils are subject to flutter motion. This mode is not present in the isolated blade analysis. A plausible reason for this may be a coupling of the mode with the tower and shaft mode, which makes the mode negative damped at a lower relative wind speed in the entire turbine analysis.

The relative wind speed for a turbine in normal power producing operation is between 90 m/s and 100 m/s. Compared to this, the flutter instability is found at about twice the operational speed of the wind turbine.

Analysis without steady state downwind blade deflection

To study the effect of the downwind steady state blade deflection due to the incoming wind, an analysis was performed for an entire turbine without this effect present. The blades are thus assumed to vibrate around an undeflected state. The
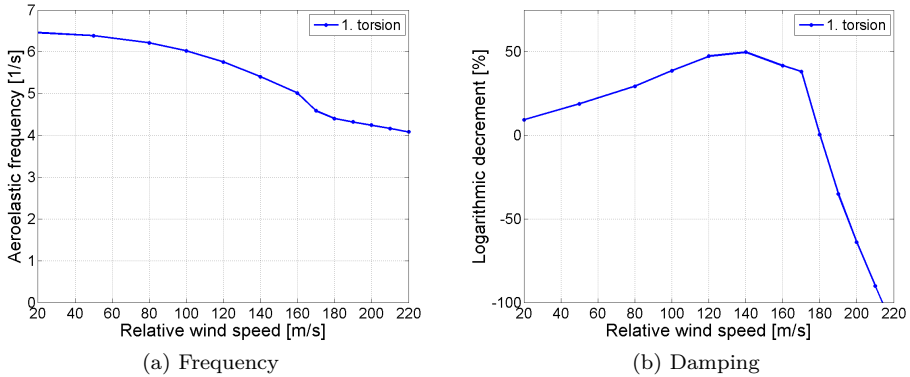
Figure 6.5: Stability analysis of the entire turbine with baseline blades without including steady state deflection of the blades

mode which became unstable in this analysis is found in figure 6.5. The mode is the 1. torsional mode and is found to become unstable at a relative wind speed of 180 m/s. This result can be compared to the analysis which includes steady state blade deflection in figure 6.3. In the analysis with steady state deflection, there are two modes which become unstable, compared to only one when the deflection is neglected. This indicates that one of the modes, probably the 3. flapwise mode becomes unstable due to the steady state deflection of the blade. This may be due to the deflection causing a coupling with torsional motion. The other mode which becomes unstable is similar to the mode in the analysis without deflection. Both the frequency and damping of these modes are similar. There are however some differences: The mode which becomes unstable when analysing without deflection is the 1. torsional mode whereas the mode which becomes unstable when including deflection is the 3. edgewise mode. This indicates that the steady state deflection of the blades may be a reason for the 3. edgewise mode to become unstable. This effect is uncertain and not understood, as there is little steady deflection of the blade at low relative wind speed. But there may be some geometrical coupling of the edgewise mode with torsion as the blade deflecte downwind. In the analysis where the steady state deflection is neglected, the critical flutter speed is found to be lower than when the deflection is present, which indicates that the critical flutter speed increase somewhat with increasing incoming wind speed. This analysis correspond to the use of the aeroelastic stability tool HAWCStab, which is a more validated tool than HAWCStab2.

Turbine in normal power producing operation

An aeroelastic stability analysis was performed for a wind turbine in normal power producing condition. The results from this analysis can be found in figure 6.6. The
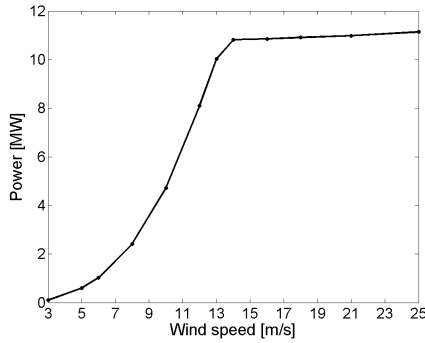
(a) Power
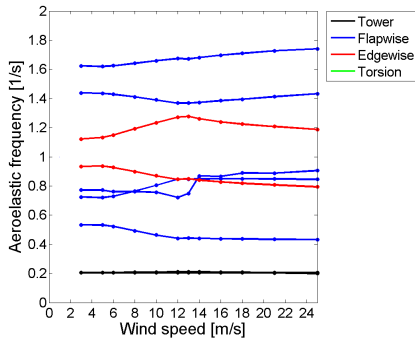
(b) Frequency
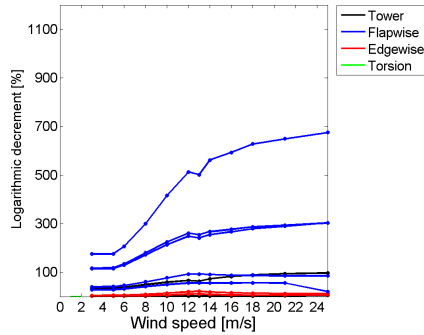
(c) Damping

Figure 6.6: Stability analysis of turbine in normal operation with baseline blades

results are plotted against the wind speed and not against the relative wind speed, as the relative wind speed is quite constant after the blades start to pitch. The pitch of the blades is controlled by the control system to achieve the desired power output at a given wind speed. The control system is further described in chapter 4.3. The wind turbine did not become unstable, in the normal operating condition. This result indicates that the wind turbine is able to produce power without having the risk of flutter instabilities.

6.1.3 Simulations in the time domain

Run-away of turbine

To study the response of the wind turbine, simulations in the time-domain were performed. First a turbine run-away was simulated. This is a situation where the power grid falls out and the generator looses its counter torque. There is thus nothing to withstand the acceleration of the rotor, until the rotational speed in high

(a) Rotational speed

(b) Relative wind speed at blade tip

(c) Flapwise

(d) Torsion
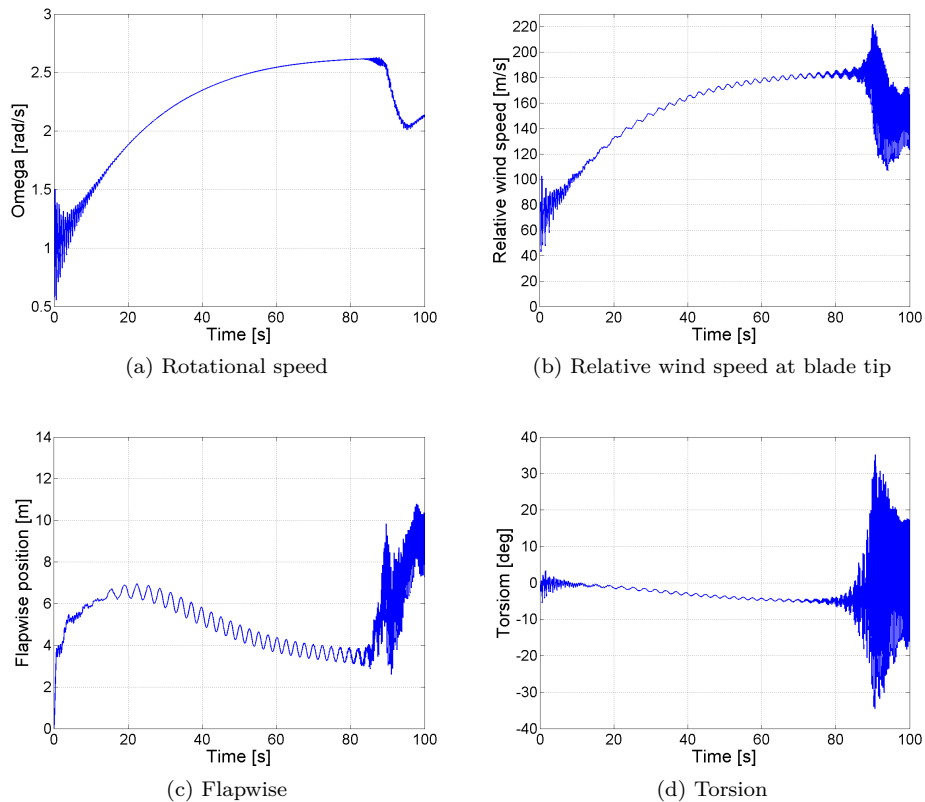
Figure 6.7: The dynamics of the rotor when the load has fallen away, baseline blades

enough for the aerodynamic drag forces to balance the lift forces. The results from the simulations of the run-away situation is found in figure 6.7. The simulation is performed with an uniform incoming wind with a wind speed of 10 m/s.

Before the instability occurs, the turbine behaves as expected in a run-away scenario. The wind speed is constant and the rotational speed is increasing as there is nothing to withhold it. The flapwise motions first increase slightly then it decreases due to the decreasing angle of attack and the increasing centrifugal forces. The blades thus do not hit the tower, before the instability occurs. It is plausible that the blades are not destroyed by the centrifugal forces before the instability occurs.

The instability of the blade happens at a relative wind speed slightly above 180 m/s. The blade then uses 20 seconds to reach significant amplitude of the blade vibrations. When the amplitude of the torsional vibrations becomes too high, the blades reach the stall area, and the amplitude of the vibrations do not increase any more. The vibrations in the torsional and flapwise direction are dominant, but

edgewise vibrations are also present.

It is plausible that the instability in the run-away situation is the flutter instability which was found in the aeroelastic stability analysis. In the stability analysis, the flutter mode has slightly positive damping at a relative wind speed of 190 m/s and negative damping at a rotational speed of 200 m/s. This indicates that the wind turbine becomes unstable at a relative wind speed between 190 and 200 m/s. In the simulation of the run-away the instability occurs at a relative wind speed slightly above 180 m/s. This corresponds to a 5 to 10 % lower relative wind speed. In the stability analysis, the wind speed is also increased when the rotational speed increases, causing a downwind deflection of the blade. There is no big deflection present in the run-away simulation as the wind speed is constant 10 m/s. In the aeroelastic stability analysis where the steady state downwind deflection is not included, the critical flutter speed is lower. In that stability analysis the critical flutter speed is 180 m/s and thus the same as in the run-away simulation. This is expected as there is litle deflection of the blade in the run-away simulation. The frequency of the vibrations is approximately 3.5 Hz in this simulation, but according the stability simulation the frequency of the mode which becomes negatively damped is 5.1 Hz. The difference may be due to the vibrations of other modes.

The wind turbine uses 80 seconds to reach the instability area. As an instability is present, causing violent vibrations, it is plausible that the wind turbine will get destroyed in a run-away situation if allowed to run to the instability. In reality there would be time to pitch the blades before the blades get destroyed by flutter, if this mechanism is still working. Should this blade be used on a wind turbine, it would be desirable to have a pitch system which has redundancy and is able to operate in a run-away situation.

Simmulations of run-away with realistic wind

Wind configuration	Relative wind speed where instability occurs
Uniform wind	180
With wind shear	180
With turbulence	165
With tower shadow	160
With wind shear and tower shadow and turbulence	160

Table 6.1: Relative wind speed where instability occurs at different wind configurations in a run-away simulation

The run-away simulations were performed with uniform wind speed. To study if the blade became unstable at a lower relative wind speed in a more realistic incoming wind, the same simulation was performed with realistic wind conditions. Different effects were added one at the time. First a simulation was performed with wind shear. Second a simulation was performed with turbulent wind with

a turbulence intensity of 10 %. Then a simulation was performed with the tower shadow effect. Finally a simulation was performed with all these effects together. The relative wind speed where the different cases became unstable can be found in table 6.1. The results show that the wind shear has little influence on when the blade becomes unstable. When the tower shadow effect is added, there is an effect. The wind turbine becomes unstable at a relative wind speed around 160 m/s, which is lower than in the simulations without tower shadow. A plausible reason is that the tower shadow results in a change of the angle of attack on the blade, which can cause instabilities at a lower relative wind speed. When turbulence is added, there is also an effect and the instability occurs at 165 m/s. When all the effects are present, the instability happens at a relative wind speed of 160 m/s, which is the same as when only the tower shadow effect is present. These simulations show that the tower shadow effect and the turbulence are able to create instability at a lower wind speed. The effect of the wind shear leads to too small changes on the wind turbine blades. The wind turbine in this case is upwind, and has only a limited tower shadow. A downwind rotor would have a higher effect of the tower shadow. It is possible that this could lead to an even earlier trigger of the instability.

6.2 Soft blade

To study how the instabilities is dependent on the blade stiffness, a softer blade was studied. The soft blade is a blade which typically would be used on a downwind wind turbine, where there is no risk of the blade hitting the tower when the blades deflect downwind.

6.2.1 Aeroelastic stability analysis

An aeroelastic stability analysis was performed with the soft blade, to study which modes could cause instability of the blade. As the blade is softer the natural frequencies are lower and the deflections of the blades are bigger.

6.2.2 Modes which cause instabillity

Isolated blade

The modes which have negative damping for the soft blade can be found in figure 6.8. In the results from the analysis with a isolated blade, there are 2 modes which has negative damping. One of them becomes negative at a relative wind speed of 180 m/s, and the other at a relative wind speed of 190 m/s.

The first mode which becomes unstable is the 2. edgewise blade mode at a relative wind speed of 180 m/s. When the mode achieves negative damping, the aeroelastic frequency is 2.3 Hz. The motions of the blade when it becomes unstable are found

(a) Frequency   (b) Damping
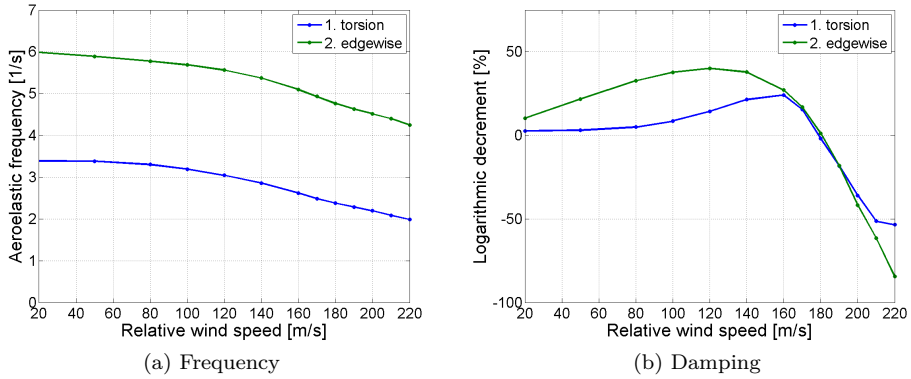
Figure 6.8: Modes which cause instabillity in the isolated blade analysis with soft blades

to be a combination of edgewise motion, torsion and flapwise motion. This is not the typical flutter motion. The reason for this instability may be an unfavourable coupling of modes. It is possible that the instability is not dependent on the relative wind speed, but rather a result of the big deflection of the blade due to the incoming wind speed.

The second mode to have negative damping is the 1. torsional mode at a relative wind speed of 190 m/s. The mode seems to become negative damped only slightly above 180 m/s. At low relative wind speeds the blade motions is purely torsional, but as the wind speed increase the torsional motion couples with flapwise motion. At high relative wind speed the modes couples to a flutter mode. The mode has the typical highly negative damping of flutter above the critical wind speed.

When comparing the results with the isolated blade analysis for the baseline blade, it is found that the mode which has flutter motion is the same as the mode, the 1. torsional mode, which couples to the flutter mode in the analysis of the baseline blade. At the soft blade the mode becomes unstable at a slightly lower relative wind speed than when the baseline blade is simulated. The other mode which has negative damping for the soft blade is not present in the stability analysis of the baseline blade, and may be due to a coupling of modes due to the lower stiffness of the blade.

Entire turbine

A stability analysis of the entire turbine was performed on the soft blade. The modes which became negatively damped is showed in figure 6.9. One mode has negative damping at a relative wind speed of 170 m/s and next mode at 180 m/s. The two next modes become unstable at 200 m/s and 210 m/s.

51

(a) Frequency   (b) Damping
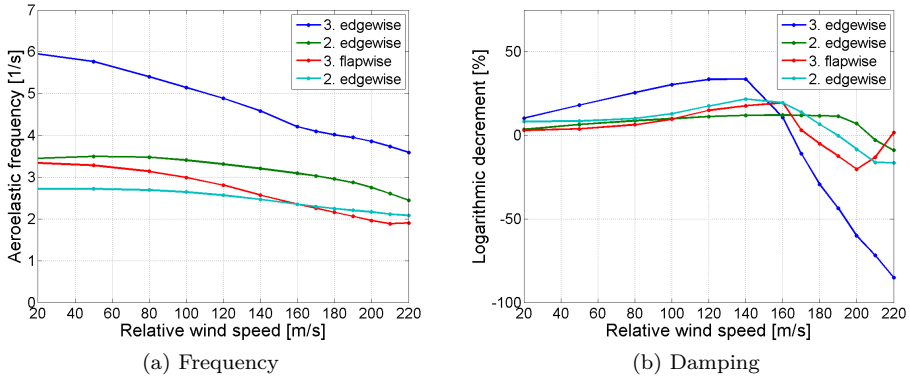
Figure 6.9: Modes which cause instabillity in the entire turbine analysis with soft blades

The mode which becomes unstable at 170 m/s is either the 1. torsion backward whirling mode or the 3. edgewise symmetric mode. It is difficult to know which of them as their frequency at low wind speeds almost coincides, and the modes are heavily coupled with each other from low wind speeds. The 1. torsion mode is the same mode which became unstable in the simulation with isolated blade. The 3. edgewise symmetric mode is the mode which became unstable in the entire turbine analysis of the baseline blade. The mode has a frequency around 6 Hz at low relative wind speeds, which decreases to 3.5 Hz at high relative wind speeds. At low wind speeds the motions are a combination of edgewise and torsional motion, but as the wind speed increase the motions become more torsional. At higher relative wind speed the motion couples with flapwise motion and the typical flutter motion is found. The flutter motion leads to a negative aeroelastic damping and thus instability of the turbine. The mode has the large levels of negative damping at high wind speeds, which is characteristic for flutter.

The mode which has negative damping at a relative wind speed of 180 m/s is the 3. flapwise backward whirling mode. It has a decreasing frequency when the relative wind speed increases, which is mainly due to the backward whirling. When it becomes unstable it has a frequency of 2.2 Hz and is found to have the typical flutter motion. After the mode has become negative damping, the damping increases again. A possible reason for this may be that not all of the airfoils are subject to flutter. This is the only mode which has this behaviour.

The 2 last modes to become instable are the 2. edgewise symmetric mode and backward whirling mode. The 2. edgewise mode is the same mode which became unstable in the isolated blade analysis. It is plausible that this instability is due to an unfavourable coupling between the edgewise bending mode with blade torsion, which causes a change in the effective direction of the blade vibrations.

In the isolated blade analysis, the 2. edgewise mode becomes unstable at slightly lower relative wind speed than the flutter mode. In the entire turbine analysis, the flutter mode becomes unstable at a lower relative wind speed. The reason for this is not known. It is uncertain if the flutter mode is the same in both the isolated blade analysis and the entire turbine analysis. There are more modes which becomes unstable in the entire turbine analysis than in the isolated blade analysis. One reason for this is the multi-blade coordinate, which causes two 2. edgewise modes in the entire turbine analysis to have negative damping. The 3. flapwise mode was not negative damped in the isolated blade analysis. A plausible reason for this is that it may be dependent on a coupling with the tower or shaft modes to become unstable. The modes become unstable at a lower relative wind speed in the analysis of the entire turbine than in the analysis of the isolated blade. This corresponds well to the results from the analysis with the baseline blade.

Compared to the results from the baseline blade there are more modes which becomes unstable for the soft blade. The first mode becomes unstable at a lower relative wind speed for the soft blade than for the baseline blade. Both the 1. torsional mode, and the 3. flapwise mode which were the first to become unstable in the analysis with soft blade is found in the analysis of the baseline blade. The instability of the 2. edgewise mode at higher relative wind speed is not found for the baseline blade. This instability may be due to the higher deflections of the soft blade.

The blade becomes unstable at aproximately 1.8 times the operational speed of the wind turbine.

Stability in normal power producing operation

To check if the wind turbine is stable in normal power producing operation, a stability analysis was performed using a control system. The control system used is the same used for the baseline blade, which is described in chapter 5.1 and in chapter 4.3. The results from this analysis are found in figure 6.6. In the stability analysis the turbine was found to be aeroelastic stable for all the operational points during normal operation.

6.2.3 Simulations in the time domain

A simulation of a turbine run-away is shown in figure 6.11. In this time-domain simulation the wind speed is uniform and constant 10 m/s. The simulation shows that the wind turbine becomes unstable at a relative wind speed of 155 m/s. The instability causes considerable flapwise and torsional vibrations, and is assumed to be flutter instability. As the vibrations increases, the stall area is reached and the amplitude of the vibrations does not increase more. In the aeroelastic stability analysis the instability occur at a relative wind speed slightly below 170 m/s in the entire turbine analysis. The 5% difference in critical flutter speed may be due
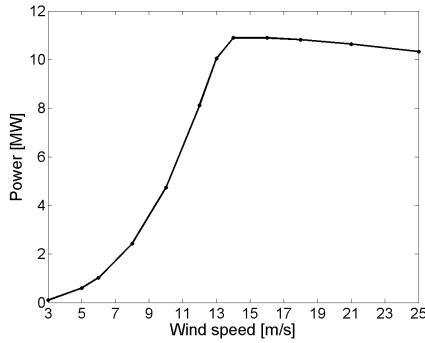
(a) Power
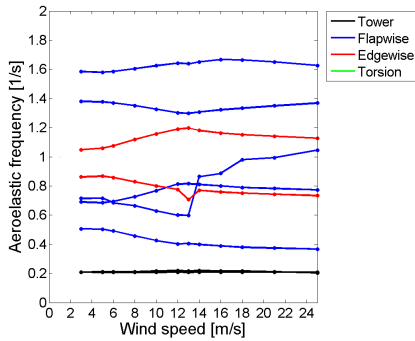
(b) Frequency
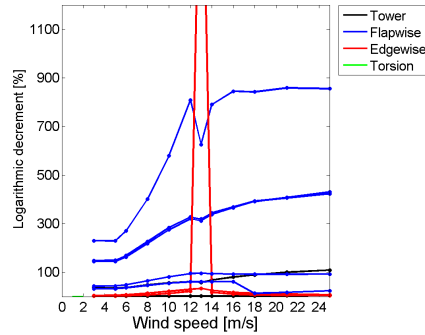
(c) Damping

Figure 6.10: Stability analysis of turbine in normal operation with soft blades. The peak in (c) is due to numerical issues in the simulation

to the lower incoming wind speed in the run-away simulation. Another element which may cause the difference in the critical flutter speed is that there are more non-linearities present in the simulation in the time domain.

The instability occurs 30 seconds into the simulation. The vibrations of the blade increases rapidly and within 5 second the torsion of the blade is ±20 degrees. This is a faster increase of the amplitudes, than in the case with the baseline blades. A reason for this may be the lower stiffness of the blades. The frequency of the vibrations are found to be approximatly 3 Hz. This is close to the frequency of 3.5 Hz of the flutter mode when it became unstable in the stability analysis. The difference may be due to the effect of the other modes present. The instability of the turbine occurs before the turbine reaches a constant run-away speed. When the results from before the instability are studied, it can be found that the blade never deflects such that it hits the tower. If the control system of the pitching of the blades is operating, it is possible to pitch the blades before the wind turbine reaches instability.

54

(a) Rotational speed

(b) Relative wind speed at blade tip

(c) Flapwise

(d) Torsion
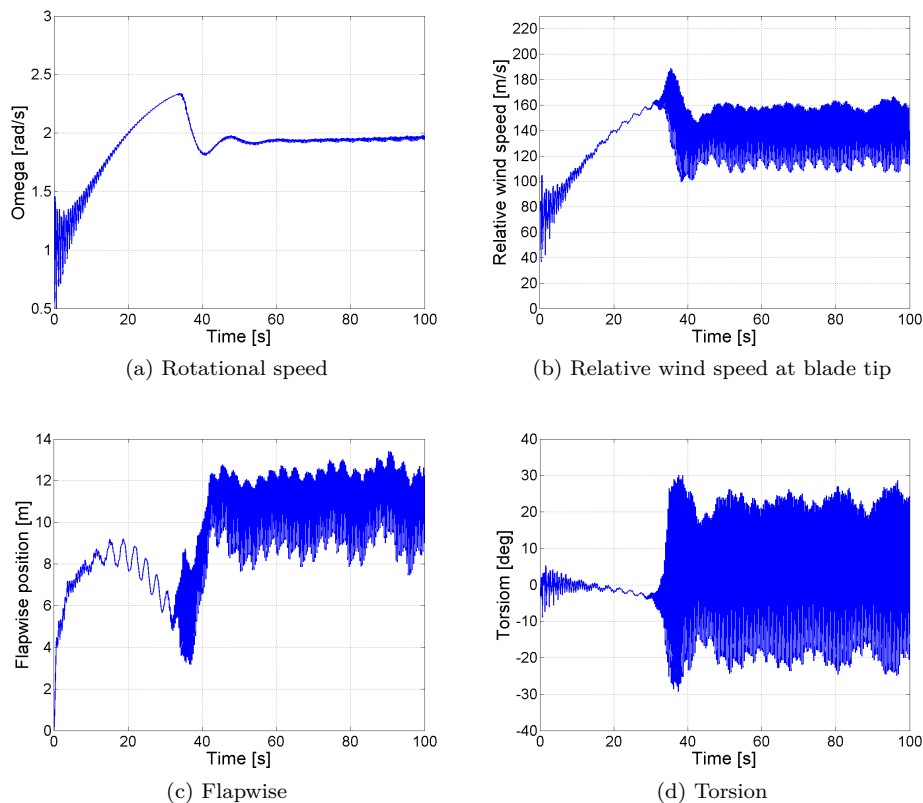
Figure 6.11: The dynamics of the rotor when the load has fallen away, soft blades

The results from the simulations on the baseline blade with realistic incoming wind indicate that the instability occurs at lower wind speeds when the effect of wind shear, tower shadow and turbulence is added to the simulation. It is plausible that this would also be the case for the soft blade. The instability would thus occur at lower relative wind speed in realistic wind conditions.

6.3 Stiff blade

A stiff blade was analysed, to study what effect an increased torsional stiffness has on the aeroelastic stability of the blade.

(a) Frequency (b) Damping
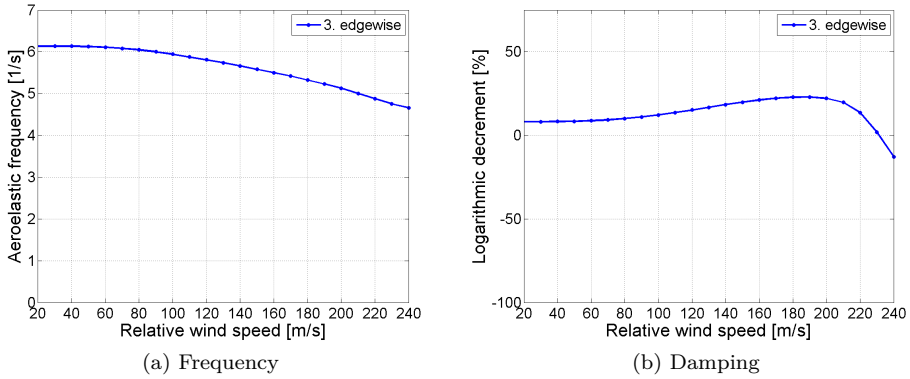
Figure 6.12: Modes which cause instabillity in the entire turbine analysis with stiff blades

6.3.1 Aeroelastc stability analysis

An aeroelastic analysis of the isolated blade was performed. It showed that at a relative wind speed of 220 m/s, no modes was yet unstable. At 240 m/s the 1. torsional mode was found to have negative damping after coupling with flapwise motion into the flutter mode.

The entire turbine was then analysed. Still no mode had negative damping at relative wind speeds of 220 m/s or below. The first mode to have negative damping is found at a relative wind speed of 240 m/s. This mode is shown in figure 6.12. The mode which becomes unstable is the 3. edgewise symmetric mode, which is the same mode to become unstable in the entire turbine analysis of the baseline blade, and not the 1. torsional mode as in the isolated blade analysis. The mode couples with torsional motion and eventually with flapwise motion to create the flutter motion. The frequency of the 3. edgewise symmetric mode is 1.5 Hz lower than the frequency of the 1. torsional modes at, but they still couple. At high wind speed it is found to have the typical flutter motion, and the steep decrease in aeroelastic damping which is typical for flutter.

Normal power producing operation of the wind turbine was also studied in figure 6.13. The wind turbine does not become unstable in normal power producing operation. The output from the control system of the baseline blade was used in this analysis.

6.3.2 Simulations in the time domain

Run-away simulation of the stiff blade was performed to study how the blade would react to loosing the power grid. The results can be found in figure 6.14.
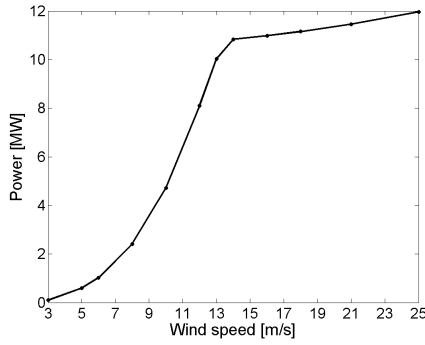
(a) Power
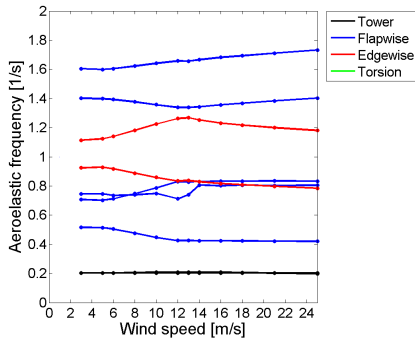
(b) Frequency
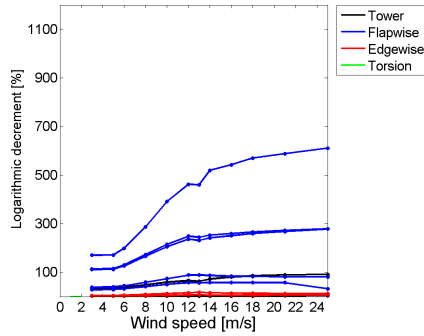
(c) Damping

Figure 6.13: Stability analysis of turbine in normal operation with stiff blades

The results show that the wind turbine is able to reach run-away speed without becoming unstable. The rotational speed increases to a constant speed of 26 rpm which corresponds to a rotational speed of 195 m/s. The flapwise motions increases slightly before it decreases as the rotational speed increases due to centrifugal forces and decreased angle of attack. The blade does thus not hit the tower. The torsion decreases slightly as the rotational speed increases.
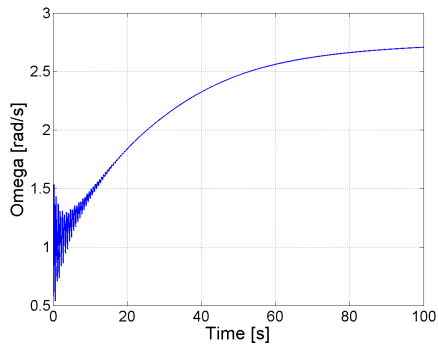
(a) Rotational speed
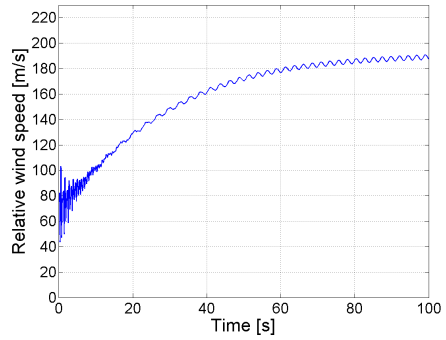
(b) Relative wind speed
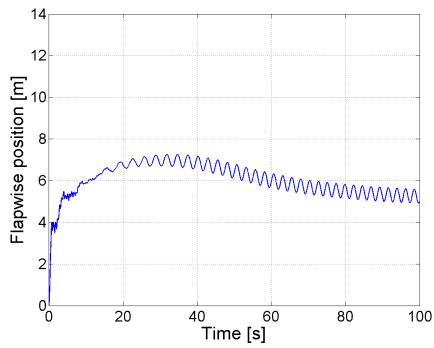
(c) Flapwise
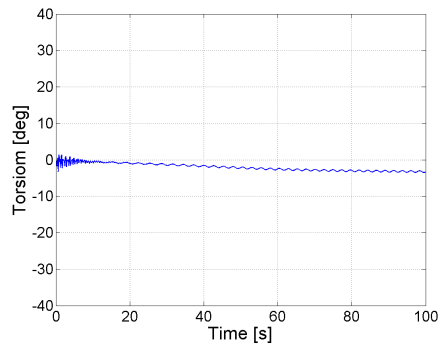
(d) Torsion

Figure 6.14: The dynamics of the rotor when the load has fallen away, stiff blades

Chapter 7

Discussion

In this thesis the aeroelastic instabilities of a 10 MW wind turbine are studied. Aeroelastic stability analyses were performed using three different blades: one baseline blade, one softer blade and one stiffer blade. The goal of the analysis was to evaluate if the turbine is prone to flutter instabilities.

The baseline blade was found to become initiate flutter instabillites at a relative wind speed slightly below 200 m/s, which is approximately twice the operational speed of the blade. Two analysis approaches were used, isolated blade analysis and entire turbine analysis. The critical flutter limit was found to be slightly higher in the isolated blade analysis. In the isolated blade analysis the 1. torsional mode became unstable and in the entire turbine analysis the 3. edgewise mode became unstable. The reason for this difference is uncertain, but it was found that the 3. edgewise symmetric mode coupled intensely with the 1. torsional mode. Only at low wind speeds was the mode found to include edgewise motion. An aeroelastic stability analysis of the entire turbine without the effect of the steady state downwind deflection of the blades was also performed. This analysis indicated that the deflection of the blades might be an element in causing the 3. edgewise mode to become unstable. It also indicated that the critical flutter speed may increase with increasing downwind deflection. It was concluded that the wind turbine did not become unstable in normal power producing operation.

Simulations of the wind turbine in the time domain were also performed to study the response of the turbine and to validate the stability analysis. A run-away situation was simulated, where the wind turbine accelerates until a constant rotational speed is reached where the drag forces balances the lift forces. The wind turbine became unstable before the constant run-away speed was reached, when the relative wind speed was 180 m/s. This indicates a critical wind speed which is around 8% lower than in the stability analysis. A plausible reason for this is that the downwind deflection of the blades is lower in the run-away simulation than in the stability analysis, due to lower wind speed. Stability analysis with higher

incoming wind speed may thus not be conservative, particularly the isolated blade analysis. In a run-away situation it is possible to avoid the instability by pitching the blades, if this mechanism still works. In this simulation it would be time to pitch the blades before the instability occur. The turbine run-away was also simulated with more realistic wind conditions. It was found that the turbulence and the tower shadow effect on the wind field may cause the turbine to become unstable at a lower relative wind speed, due to changes in the angle of attack.

The turbine was then analysed with soft blades. The blades are typical blades for a downwind wind turbine. The turbine was found to become unstable with flutter at a relative wind speed of 170 m/s, in the entire turbine analysis. This is a lower relative wind speed than in the analysis of the baseline blade, as the lower stiffness enables an easier coupling of the modes into the flutter mode. In this analysis it is difficult to conclude if it is the 3. edgewise mode or the 1. torsional mode which became negative damped. Time domain simulations were performed, and the results corresponded well with the results from the stability analysis. The difference of critical wind speed between the stability analysis and the time simulations are around 5 %, due to the same considerations as for the baseline blade. The soft blade is a typical downwind blade. In a downwind position, the effect of the tower shadow is increased. This may lead to flutter instability at a lower relative wind speed.

A turbine with stiff blades was also studied. The blade had the same stiffness in edgewise and flapwise direction as the baseline blade, but was stiffer in torsional direction. The turbine with this blade became unstable with flutter at a relative wind speed of 240 m/s, which is more than twice the operational speed of the turbine. It was the 3. edgewise mode which becomes unstable in the entire turbine simulation, as in the baseline simulation. The stiff blade does not become unstable in normal power producing operation and is able to reach the run-away speed without any flutter instability in a run-away situation.

The same mode was found to first become unstable for all three blades. The turbine became unstable at different relative wind speeds, due to the different stiffness of the blades. The soft blade became unstable at the lowest wind speed and the stiff blade at the highest wind speed. In this thesis none of the blades experience aeroelastic instabilities in normal power producing operation. But the baseline and soft blade was found to become unstable in a run-away situation of the turbine. If it is a requirement that the turbine should be able to survive a run-away situation it is important to have a high enough torsional stiffness to avoid flutter, and the baseline and soft blade should thus not be used.

As no other stability analyses has been performed on this wind turbine or wind turbines with similar size, there are no articles which can be used to verify the critical flutter speed. But for the NREL 5 MW reference turbine, several aeroelastic stability studies has been performed. In a study by Hansen [2] the NREL turbine is found to be unstable at rotational speeds exceeding 25 rpm in an entire turbine simulation where the steady state deflection of the blade is neglected. 25 rpm

corresponds to a relative wind speed of 165 m/s, as the radius of the blade is 63 m. This is approximately twice the operational speed of the turbine. When the steady state deflection is neglected, the baseline in this thesis was found to become unstable at 1.8 times the operational speed at a relative wind speed of 180 m/s. There was not found any studies that indicated that the NREL turbine is prone to flutter in a run-away simulation. In the aeroelastic analysis of the NREL turbine, the 3. flapwise mode becomes negative damped. This mode is found to become unstable in the analysis of the baseline blade and the soft blade in this thesis, but not as the first mode to become unstable. It is not found indication of flutter instability for the 3. edgewise modes in any articles. Kallesøe found that the flutter speed did not change much with the steady state deflection of the blades for the NREL 5 MW wind turbine. In this study it was found that the critical flutter speed varied somewhat with steady state the deflection of the blade. The difference may be due to different blades being studied with different tools.

In this thesis a new aeroelastic simulation tool, HAWCStab2, is used. Version 97 of the program is used in this thesis. There exists little validation of this tool, as it is new. The time domain simulations and the input to HAWCStab2 were validated against other codes and the results corresponded well. No experimental data for modern commercial turbines are able for validation of predicted flutter limits.

Chapter 8

Conclusion and Further Work

8.1 Conclusion

In this thesis a 10 MW wind turbine was studied to investigate if it was prone to flutter. Three different analyses were performed with turbines with different blades: baseline blades, blades which were softer, and blades which were stiffer in torsional direction.

The input to the aeroelastic stability tool was validated in the time domain by. The input to HAWCStab2 corresponds mainly to the input to the aeroelastic time domain tool HAWC2. Simulations in HAWC2 was performed and compared with other aeroelastic codes. The results from the different codes corresponded well. As no data for experiments on full-scale wind turbines are available, the critical flutter limits calculated are not validated.

In the aeroelastic stability analysis it was also confirmed that the isolated blade simulations may not be conservative whereas simulations with quasi-steady aerodynamics are very conservative.

It was concluded that the wind turbine and the blades studied in this thesis are not prone to flutter instabilities in normal power producing operation. The critical flutter limit is found to be around twice the operational speed for the baseline blade, which corresponds to a relative wind speed of 200 m/s. For the soft blade the critical flutter limit was found at 80 % above the operational speed and for the stiff blade at 1.4 times of the operational speed. These results assumed high incoming wind speed. In a run-away scenario, a turbine with the baseline blades or the soft blades is prone to flutter instabilities, but not a turbine with the stiff blades.

8.2 Further Work

Some objects which should be furthered studied are:

- Simulations should be performed with an updated version of HAWStab2, when the debugging phase is finished.

- In the results from the aeroelastic stability analysis, the 3. edgewise symmetric mode is found to become the flutter mode. Why this mode becomes the flutter mode should be further studied. It is also a question why it is different modes which experienced flutter in the isolated blade analysis and the analysis of the entire turbine.

- As the program which is used, HAWCStab2, is new, the program needs to be validated against other aeroelastic stability tools. If possible, the critical flutter limits should be validated against experimental results.

Bibliography

[1] D. Smith. A case study and analysis of the tacoma narrows bridge failure. *Engineering Project*, 99, 1974.

[2] M. H. Hansen. Aeroelastic instability problems for wind turbines. *Wind Energy*, 10(6), 2007.

[3] M. H. Hansen. Aeroelastic stability analysis of wind turbines using an eigenvalue approach. *Wind Energy*, 7(2), 2004.

[4] Lars Frøyd and Ole G. Dahlhaug. Rotor design of a 10 MW offshore wind turbine. 2011.

[5] Y. C. Fung. *An Introduction to the Theory of Aeroelasticity*. Courier Dover Publications, May 2002.

[6] T. Theodorsen and NACA. Langley Research Center. General theory of aerodynamic instability and the mechanism of flutter. Technical report, National Advisory Committee for Aeronautics, 1935.

[7] D. W Lobitz and P. S Veers. Aeroelastic behavior of twist-coupled HAWT blades. In *ASME/AIAA Wind Energy Symposium, Reno, NV*, 1998.

[8] D. W Lobitz. Aeroelastic stability predictions for a MW-sized blade. *Wind Energy*, 7(3), 2004.

[9] B. Kirchgässner. ARLIS-A program system for aeroelastic analysis of rotating linear systems. In *Proceedings of the European Wind Energy Conference*, 1984.

[10] J. T Petersen, H. A Madsen, A. Bjørck, P. Enevoldsen, S. Øye, H. Ganander, and D. Winkelaar. *Prediction of dynamic loads and induced vibrations in stall*. Ris\o National Laboratory, 1998.

[11] P. K. Chaviaropoulos, N. N. Soerensen, M. O.L Hansen, I. G. Nikolaou, K. A. Aggelis, J. Johansen, M. Gaunaa, T. Hambraus, H. F von Geyr, C. Hirsch, et al. Viscous and aeroelastic effects on wind turbine blades. the VISCEL project. part II: aeroelastic stability investigations. *Wind Energy*, 6(4), 2003.

[12] P. Chaviaropoulos, E. S. Politis, N. N. Sørensen, M. H. Hansen, B. H. Bulder, D. Winkelaar, D. A. Saravanos, T. Philippidis, C. Galiotis, M. O. Hansen, et al.

Recent advances on damped wind turbine rotor blades, the DAMPBLADE project. In *Proceedings of the European Wind Energy Conference 2003*, 2003.

[13] T. J Larsen, H. A Madsen, A. M Hansen, and K. Thomsen. Investigations of stability effects of an offshore wind turbine using the new aeroelastic code HAWC2. In *Proceedings of the conference Copenhagen Offshore Wind*, 2005.

[14] J. M Jonkman and M. L Buhl Jr. FAST user's guide. *National Renewable Energy Laboratory, Rept. NREL/EL-50-29798, Golden, Colorado*, 2004.

[15] D. W Lobitz. Parameter sensitivities affecting the flutter speed of a MW-sized blade. *Journal of Solar Energy Engineering*, 127, 2005.

[16] B. S. Kallesøe. Effect of steady deflections on the aeroelastic stability of a turbine blade. *Wind Energy*, 2010.

[17] M. H. Hansen. Aeroelastic properties of backward swept blades. AIAA-2011-260, Orlando, Florida, January 2011. AIAA.

[18] P. Fuglsang. Aeroelastic stability and control of large wind Turbines-STABCON. In *Proceedings of the 2003 European Wind Energy Conference and Exhibition, Madrid, Spain*, 2003.

[19] V. A. Riziotis, S. G. Voutsinas, E. S. Politis, and P. K. Chaviaropoulos. Aeroelastic stability of wind turbines: the problem, the methods and the issues. *Wind Energy*, 7(4), 2004.

[20] T. van Engelen. Control design based on aero-hydro-servo-elastic linear models from TURBU (ECN). In *Proceedings of the European Wind Energy Conference*, 2007.

[21] M. H. Hansen. Improved modal dynamics of wind turbines to avoid stall-induced vibrations. *Wind Energy*, 6(2), 2003.

[22] J. J. Thomsen. *Vibrations and Stability: Advanced Theory, Analysis, and Tools*. Springer Verlag, 2003.

[23] B. S. Kallesøe. A low-order model for analysing effects of blade fatigue load control. *Wind Energy*, 9(5):421–436, 2006.

[24] J. J Bertin and M. L Smith. *Aerodynamics for engineers*. Prentice Hall New Jersey, 2002.

[25] J. F Manwell, J. G McGowan, and A. L Rogers. *Wind energy explained*, volume 1. Wiley Online Library, 2002.

[26] M. H Hansen, M. Gaunaa, and H. A Madsen. A Beddoes-Leishman type dynamic stall model in state-space and indicial formulations. *Risø1354 (EN)*, 2004.

[27] T. J. Larsen. Hawc2 course material, 15-17.03.2011.

[28] T. J. Larsen. How 2 hawc2, the users manual. Technical report, Risø DTU National Laboratory for Sustainable Energy, 2009.

[29] Lars Frøyd and Ole G. Dahlhaug. A conseptual design method for parametric study of offshore wind turbines. 2011.

[30] P. Passon, M. Kühn, S. Butterfield, J. Jonkman, T. Camp, and T.J Larsen. OC3-benchmark exercise of aero-elastic offshore wind turbine codes. In *Journal of Physics: Conference Series*, 2011.

Appendix A

Analysis of turbine with working generator
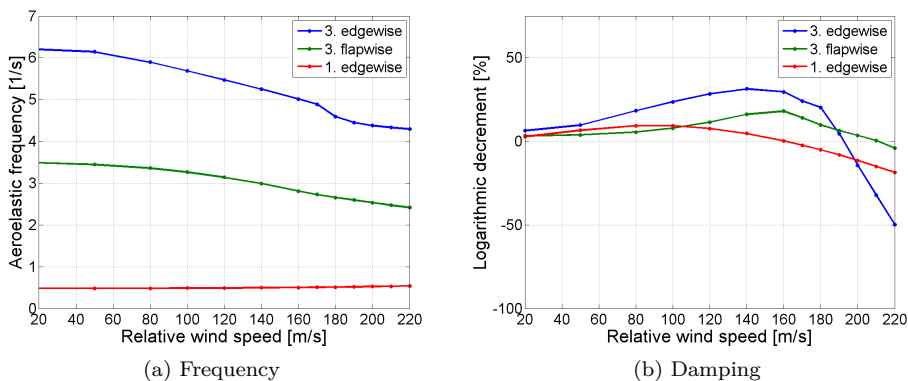
Figure A.1: Modes which cause instability in the entire turbine analysis with fixed bearing

In the input to the aeroelastic stability analyses in this thesis, the bearing between the shaft and the tower was set to be free. If this bearing is set to fixed, the 1. edgewise mode corresponds to the 1. fixed-free drive train torsion. When the wind turbine is working in reallity this mode is present when the generator functions properly. An aeroelastic stability analysis of this situation is were performed and the modes which became unstable is found in figure A.1. The first egdewise symmetric mode is found at a low frequency and is found to become negative damped at a relative wind speed of 170 m/s. The negative damping is probably due to unfavourable coupling with the torsional bending modes and the tower modes, due to the large deflection of the blade.
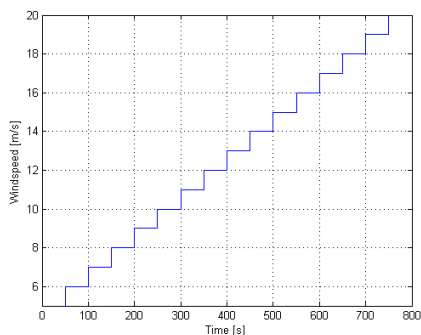
Figure A.2: Wind speed

Simulations were run in the time domain where the generator was assumed to be working properly. Different simulations were run with constant rotational speed and increasing wind speed. Some of these are found in figure A.3. The wind turbine was found to be unstable at all simulated wind speeds when the rotation caused a relative wind speed of 185 m/s. The vibrations were mainly torsional, and it is assumed that the critical flutter limit is reached at this relative wind speed. This result confirms the result from the run-away simulation that the critical flutter speed is slightly above 180 m/s.

At low rotational speeds and high wind speeds an instability was found which caused flapwise-edgewise vibrations. The growth of the amplitudes was slow compared to the flutter vibration and the frequency of the vibrations was lower. As the rotational speed is set to be constant in the simulations the results are comparable to stability results with a fixed bearing between the tower and the shaft. When a fixed bearing is present, the 1. edgewise symmetric mode becomes unstable at a relative wind speed of 170 m/s. It is possible that this instability is due to the downwind deflection of the blades due to the high incoming wind speed.
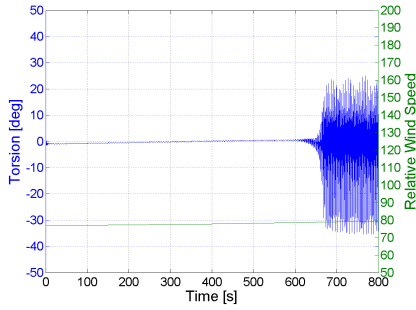
(a) Torsional rotation at 10 rpm
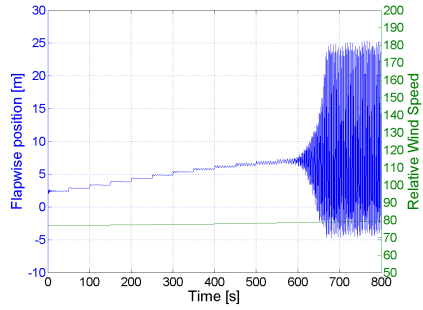
(b) Flapwise motion at 10 rpm
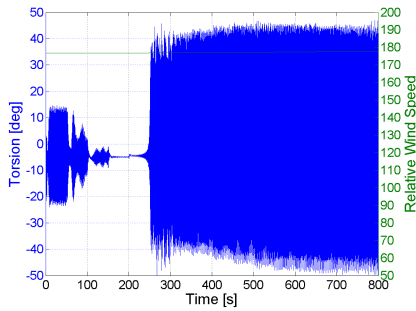
(c) Torsional rotation at 24 rpm
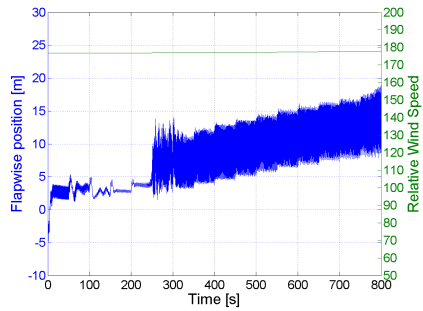
(d) Flapwise motion at 24 rpm
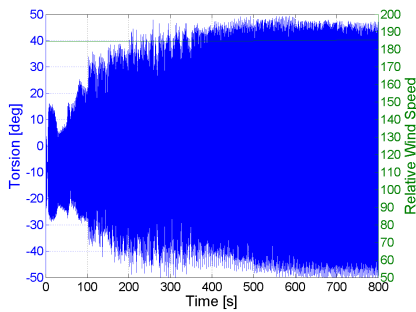
(e) Torsional rotation at 25 rpm
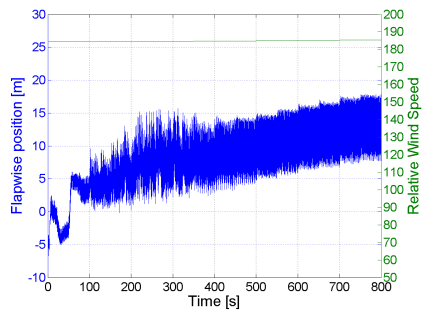
(f) Flapwise motion at 25 rpm

Figure A.3: The wind turbine with increasing wind speed at different rotational speeds

Appendix B

HAWCStab2 version 98

A new version of HAWCStab 2 is beeing released 09.06.2011, after some bugs were found in version 97, which is the version used in this thesis. A note from the designer of the tool HAWCStab2, Morten Hartvig Hansen, describing the bug correction is found in section B.1

The modes which becomes unstable in the result for an entire turbine analysis of the baseline blade in the new version is found in figure B.1. In figure B.2, the result from version 97 is showed, to compare against.

The same modes are found to become unstable in both version of the tool. It is still the 3. edgewise mode which becomes first unstable at a relative wind speed of 200 m/s in the new version. But in the new version the other mode to become unstable, the 3. flapwise mode becomes unstable at a lower relative wind speed than in version 97. It also has negative aeroelastic damping at a relative wind speed of 200 m/s, and it is possible that it becomes unstable slightly before the 3. edgewise mode.

So in general there are small differences between the versions. The wind turbine becomes unstable at the same relative wind speeds, and the same modes are present.
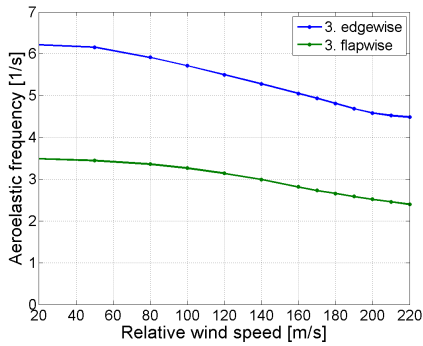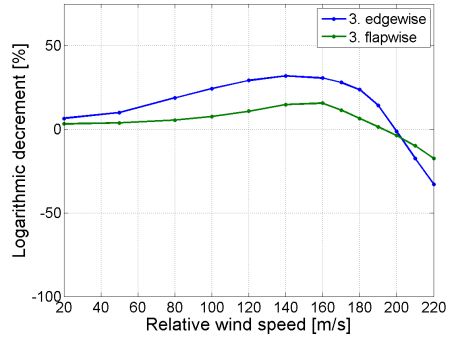
(a) Frequency   (b) Damping

Figure B.1: Modes which cause instability in the entire turbine analysis with the baseline blades version 98
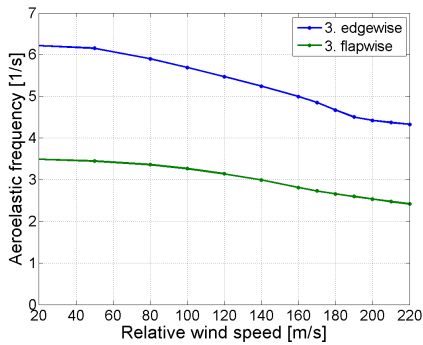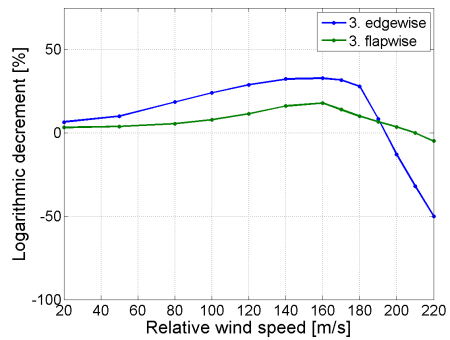
(a) Frequency   (b) Damping

Figure B.2: Modes which cause instability in the entire turbine analysis with the baseline blades version 97

B.1   Note from Morten Hartvig Hansen

Bug corrections from HAWCStab2 revision 97 to 98:

Two main bugs have been corrected (more details given below):

1. Bug in the setup of the modal expansion matrix used for expanding the structural DOFs to condition the eigenvalue problem has been corrected. It has meant that mode shapes involving cyclic rotor DOFs were distorted if the user pressed the "Apply" button in the sorting dialog box. It may have had a minor impact on the eigensolutions themselves due to worse conditioning of the problem.
2. Aerodynamic stiffness terms have been added in the linearization of the aerodynamic forces. These terms were neglected in the previous reversions due to the assumption that they were small and some implementation problems for the coupling terms between rotor support DOFs (tower and shaft/nacelle) and rotor DOFs. These terms will have the largest effect on the aeroelastic behaviour of modes involving blade motions when the blades are largely deflected.

Ad. 1: The modal expansion matrix used for conditioning the eigenvalue problem in HAWCStab2 is setup by the undamped standstill modes of each body of the tower, nacelle/shaft, and blades that are be separated by bearings. This approach is different from the modal matrix used in the old HAWCStab where the undamped standstill modes of the entire turbine were used which cannot to handle the bearings. The bug in revision 97 was a "copy and paste" error during the coding process, where the undamped standstill modes of the cyclic/asymmetric rotor DOFs (cosine and sine components of the multi-blade coordinates) are inserted into the modal expansion matrix in the reversed order. The underlined code in the following code section is the bug and has been deleted:

```
do j=1,n ! eigenvalues and eigenvectors in decreasing order from dgvcsp
  do i=1,n
    phi_mat(  i+n1-1-noffset, j+n1-1-noffset)=evecs(i,j)
    if ((isubs.eq.3).and.(.not.blade_only)) then
      phi_mat(i+n1-1-noffset+  ndofs_rotor, j+n1-1-noffset+ndofs_rotor)=evecs(i,n+1-j)
      phi_mat(i+n1-1-noffset+2*ndofs_rotor, j+n1-1-noffset+2*ndofs_rotor)=evecs(i,n+1-j)
    endif
  enddo
enddo
```

Ad. 2: The previously neglected contributions to the aerodynamic stiffness matrix are the linear generalized forces on the DOFs due to their movement of the steady state force. They are included in the description of the blade only model in Eq. (33) of [1], but were removed in the previously released versions (< rev. 98), because they were considered small and due to problems in the derivations of the coupling terms between rotor support DOFs (tower and shaft/nacelle) and rotor DOFs, and therefore not for the blade only analysis. These problems have been resolved in revision 98. The largest effect of the new terms will be on blades with large deflections, mostly on the coupling between edgewise blade bending and its torsion.

[1] Hansen, M. H., "Aeroelastic properties of backward swept blades", In the Proceedings of 49th AIAA Aerospace Sciences Meeting Including The New Horizons Forum and Aerospace Exposition, Orlando, 4-7 January, 2011.

Morten Hartvig Hansen
Risø-DTU, Roskilde, June 9, 2011

x

Appendix C

Input to HAWCStab2

C.1 Blade definition file

4 Nset

---

r	m	x_cg	y_cg	ri_x	ri_y	x_sh	y_sh	E	G
$1	39								
0	9.45E+02	-9.52E-06	-2.03E-06	1.2301	1.2251	-9.52E-06	-2.03E-06	1.02E+10	2.13E+09
1.38E+00	9.50E+02	3.84E-03	6.80E-05	1.2296	1.243	3.84E-03	6.80E-05	8.68E+09	1.82E+09
2.84E+00	8.50E+02	1.64E-02	3.13E-04	1.2235	1.2947	1.64E-02	3.13E-04	9.65E+09	2.03E+09
4.29E+00	7.21E+02	3.99E-02	3.20E-03	1.1795	1.2894	8.78E-02	1.25E-03	8.84E+09	1.99E+09
5.75E+00	6.20E+02	9.02E-02	5.25E-03	1.1425	1.3307	1.77E-01	1.97E-03	9.30E+09	1.74E+09
7.21E+00	5.77E+02	1.52E-01	7.25E-03	1.0942	1.3637	2.73E-01	2.57E-03	9.81E+09	1.58E+09
8.67E+00	5.50E+02	2.08E-01	9.17E-03	1.0329	1.4033	3.64E-01	3.02E-03	1.03E+10	1.47E+09
1.01E+01	5.29E+02	2.55E-01	1.10E-02	0.9684	1.4374	4.32E-01	3.63E-03	1.06E+10	1.39E+09
1.16E+01	5.14E+02	3.06E-01	1.27E-02	0.9078	1.4667	5.26E-01	3.59E-03	1.13E+10	1.34E+09
1.31E+01	4.97E+02	3.49E-01	1.45E-02	0.8504	1.4985	6.18E-01	3.43E-03	1.20E+10	1.30E+09
1.45E+01	4.92E+02	3.70E-01	1.62E-02	0.7796	1.4806	6.38E-01	4.19E-03	1.32E+10	1.38E+09
1.60E+01	4.74E+02	3.71E-01	1.19E-02	0.7167	1.4721	6.65E-01	-1.90E-03	1.38E+10	1.40E+09
1.74E+01	4.53E+02	3.84E-01	5.18E-03	0.6648	1.4552	7.18E-01	-1.17E-02	1.55E+10	1.45E+09
1.89E+01	4.48E+02	4.00E-01	-7.71E-03	0.6154	1.4308	7.60E-01	-2.87E-02	1.70E+10	1.52E+09
2.03E+01	4.32E+02	4.13E-01	-2.02E-02	0.5708	1.3959	7.83E-01	-4.54E-02	1.92E+10	1.63E+09
2.28E+01	4.20E+02	4.03E-01	2.05E-03	0.5081	1.3691	7.86E-01	-1.96E-02	1.94E+10	1.68E+09
2.52E+01	4.06E+02	3.81E-01	3.15E-02	0.4575	1.3321	7.55E-01	1.54E-02	1.96E+10	1.73E+09
2.76E+01	4.03E+02	3.78E-01	5.64E-02	0.4158	1.2789	7.36E-01	4.43E-02	2.07E+10	1.85E+09
3.01E+01	3.90E+02	3.61E-01	7.47E-02	0.3788	1.2307	7.06E-01	6.58E-02	2.11E+10	1.93E+09
3.25E+01	3.82E+02	3.72E-01	8.62E-02	0.349	1.1753	7.11E-01	7.92E-02	2.23E+10	2.02E+09
3.49E+01	3.58E+02	3.53E-01	8.93E-02	0.3215	1.1252	6.78E-01	8.43E-02	2.25E+10	2.07E+09
3.74E+01	3.31E+02	3.28E-01	8.99E-02	0.2975	1.0792	6.41E-01	8.65E-02	2.23E+10	2.08E+09
3.98E+01	3.02E+02	3.01E-01	8.89E-02	0.2766	1.036	6.02E-01	8.67E-02	2.19E+10	2.07E+09
4.22E+01	2.73E+02	2.81E-01	8.70E-02	0.2592	0.992	5.70E-01	8.56E-02	2.17E+10	2.06E+09
4.47E+01	2.35E+02	2.49E-01	8.44E-02	0.2432	0.9593	5.32E-01	8.35E-02	2.05E+10	1.95E+09
4.71E+01	2.03E+02	2.21E-01	8.22E-02	0.2298	0.9119	4.84E-01	8.20E-02	2.00E+10	1.88E+09
4.95E+01	1.72E+02	2.03E-01	7.92E-02	0.2178	0.8764	4.62E-01	7.91E-02	1.94E+10	1.79E+09
5.20E+01	1.48E+02	1.71E-01	7.55E-02	0.2059	0.8513	4.22E-01	7.56E-02	1.76E+10	1.69E+09
5.44E+01	1.31E+02	1.35E-01	7.15E-02	0.1947	0.8289	3.71E-01	7.18E-02	1.55E+10	1.61E+09
5.64E+01	1.17E+02	1.00E-01	6.82E-02	0.1854	0.8113	3.17E-01	6.85E-02	1.33E+10	1.52E+09
5.85E+01	1.03E+02	6.86E-02	6.40E-02	0.1741	0.7784	2.55E-01	6.41E-02	1.13E+10	1.47E+09
6.05E+01	8.95E+01	3.88E-02	5.95E-02	0.1612	0.731	1.76E-01	5.92E-02	9.51E+09	1.43E+09
6.26E+01	7.92E+01	3.22E-02	5.42E-02	0.1477	0.6721	1.49E-01	5.37E-02	9.19E+09	1.46E+09
6.46E+01	6.36E+01	1.28E-02	4.46E-02	0.1312	0.5969	1.25E-01	4.58E-02	1.07E+10	1.50E+09
6.53E+01	5.88E+01	1.40E-02	4.17E-02	0.123	0.5586	1.17E-01	4.29E-02	1.12E+10	1.57E+09
6.60E+01	5.30E+01	1.52E-02	3.82E-02	0.1129	0.5115	1.08E-01	3.93E-02	1.18E+10	1.65E+09
6.67E+01	4.56E+01	1.62E-02	3.37E-02	0.0996	0.45	9.55E-02	3.46E-02	1.27E+10	1.78E+09
6.73E+01	3.57E+01	1.66E-02	2.72E-02	0.0806	0.3628	7.76E-02	2.79E-02	1.42E+10	2.01E+09
6.80E+01	2.53E+01	1.52E-02	2.00E-02	0.0596	0.2669	5.77E-02	2.06E-02	1.65E+10	2.34E+09

----

l_x	l_y	l_p	k_x	k_y	A	pitch	x_e	y_e
1.68E+00	1.66E+00	3.38E+00	0.5	0.5	1.11E+00	-4.22E+01	-9.52E-06	-2.03E-06
1.90E+00	1.94E+00	3.89E+00	0.5	0.5	1.26E+00	3.77E+01	3.84E-03	6.80E-05
1.55E+00	1.74E+00	3.31E+00	0.5	0.5	1.04E+00	1.83E+01	1.64E-02	3.13E-04
1.64E+00	1.63E+00	2.48E+00	0.5	0.5	1.05E+00	-4.33E+01	8.78E-02	1.25E-03
1.38E+00	1.37E+00	2.30E+00	0.5	0.5	8.93E-01	-4.24E+01	1.77E-01	1.97E-03
1.20E+00	1.23E+00	2.16E+00	0.5	0.5	8.20E-01	3.55E+01	2.73E-01	2.57E-03
1.03E+00	1.15E+00	1.99E+00	0.5	0.5	7.68E-01	1.38E+01	3.64E-01	3.02E-03
8.74E-01	1.09E+00	1.77E+00	0.5	0.5	7.25E-01	7.45E+00	4.32E-01	3.63E-03
7.39E-01	1.01E+00	1.55E+00	0.5	0.5	6.81E-01	5.45E+00	5.26E-01	3.59E-03
6.20E-01	9.38E-01	1.32E+00	0.5	0.5	6.35E-01	4.31E+00	6.18E-01	3.43E-03
4.99E-01	8.38E-01	1.04E+00	0.5	0.5	5.99E-01	3.65E+00	6.38E-01	4.19E-03
3.99E-01	7.55E-01	8.37E-01	0.5	0.5	5.62E-01	3.36E+00	6.65E-01	-1.90E-03
3.13E-01	6.31E-01	6.86E-01	0.5	0.5	5.11E-01	3.37E+00	7.18E-01	-1.17E-02
2.54E-01	5.46E-01	5.59E-01	0.5	0.5	4.82E-01	3.61E+00	7.60E-01	-2.87E-02
2.00E-01	4.44E-01	4.44E-01	0.5	0.5	4.41E-01	3.94E+00	7.83E-01	-4.54E-02
1.52E-01	4.11E-01	3.41E-01	0.5	0.5	4.28E-01	3.24E+00	7.86E-01	-1.96E-02
1.18E-01	3.82E-01	2.70E-01	0.5	0.5	4.16E-01	2.60E+00	7.55E-01	1.54E-02
9.40E-02	3.41E-01	2.16E-01	0.5	0.5	4.06E-01	2.05E+00	7.36E-01	4.43E-02
7.44E-02	3.07E-01	1.73E-01	0.5	0.5	3.91E-01	1.60E+00	7.06E-01	6.58E-02
5.98E-02	2.62E-01	1.38E-01	0.5	0.5	3.76E-01	1.29E+00	7.11E-01	7.92E-02
4.71E-02	2.26E-01	1.10E-01	0.5	0.5	3.52E-01	1.05E+00	6.78E-01	8.43E-02
3.71E-02	1.95E-01	8.80E-02	0.5	0.5	3.26E-01	8.69E-01	6.41E-01	8.65E-02
2.93E-02	1.68E-01	7.06E-02	0.5	0.5	3.00E-01	7.25E-01	6.02E-01	8.67E-02
2.31E-02	1.40E-01	5.65E-02	0.5	0.5	2.70E-01	6.31E-01	5.70E-01	8.56E-02
1.79E-02	1.16E-01	4.50E-02	0.5	0.5	2.37E-01	5.41E-01	5.32E-01	8.35E-02
1.38E-02	8.98E-02	3.52E-02	0.5	0.5	2.03E-01	4.25E-01	4.84E-01	8.20E-02
1.07E-02	7.00E-02	2.78E-02	0.5	0.5	1.73E-01	3.99E-01	4.62E-01	7.91E-02
8.50E-03	6.15E-02	2.26E-02	0.5	0.5	1.54E-01	3.46E-01	4.22E-01	7.56E-02
6.97E-03	5.83E-02	1.88E-02	0.5	0.5	1.42E-01	2.92E-01	3.71E-01	7.18E-02
5.90E-03	5.79E-02	1.61E-02	0.5	0.5	1.34E-01	2.55E-01	3.17E-01	6.85E-02
4.74E-03	5.50E-02	1.31E-02	0.5	0.5	1.24E-01	2.36E-01	2.55E-01	6.41E-02
3.63E-03	4.98E-02	1.00E-02	0.5	0.5	1.14E-01	2.15E-01	1.76E-01	5.92E-02
2.66E-03	3.91E-02	7.32E-03	0.5	0.5	1.02E-01	2.20E-01	1.49E-01	5.37E-02
1.51E-03	2.22E-02	4.50E-03	0.5	0.5	7.44E-02	2.27E-01	1.25E-01	4.58E-02
1.19E-03	1.75E-02	3.54E-03	0.5	0.5	6.68E-02	2.28E-01	1.17E-01	4.29E-02
8.68E-04	1.27E-02	2.57E-03	0.5	0.5	5.79E-02	2.29E-01	1.08E-01	3.93E-02
5.50E-04	8.04E-03	1.62E-03	0.5	0.5	4.73E-02	2.29E-01	9.55E-02	3.46E-02
2.57E-04	3.76E-03	7.54E-04	0.5	0.5	3.39E-02	2.30E-01	7.76E-02	2.79E-02
8.88E-05	1.29E-03	2.57E-04	0.5	0.5	2.15E-02	2.32E-01	5.77E-02	2.06E-02

Table 1 (columns r – k_x)

r	m	x_cg	y_cg	ri_x	ri_y	x_sh	y_sh	E	G	I_x	I_y	I_p	k_x
#2 Shaft													
$1 2													
0	1	0	0	0	0.2	0.2	0	2.10E+11	8.08E+10	1.00E+02	1.00E+02	0.05376	0.52
5.0191	1	0	0	0	0.2	0.2	0	2.10E+11	8.08E+10	1.00E+02	1.00E+02	0.05376	0.52
‑‑‑‑‑‑‑‑‑‑													
#3 Hub													
$3 3 Uniform hub 75 ton													
0	10133	0	0	0	1.433	1.433	0	2.10E+27	8.07E+26	1.29E+00	1.29E+00	5.56E+00	5.00E-01
1	10133	0	0	0	1.433	1.433	0	2.10E+27	8.07E+26	1.29E+00	1.29E+00	5.56E+00	5.00E-01
2.4671	10133	0	0	0	1.433	1.433	0	2.10E+27	8.07E+26	1.29E+00	1.29E+00	5.56E+00	5.00E-01
‑‑‑‑‑‑‑‑‑‑													

Table 2 (columns k_y – y_e)

k_y	A	pitch	x_e	y_e
0.52	0.59		0	0
0.52	0.59		0	0
‑‑‑‑‑‑‑‑‑‑				
0.5	9.96E-01	0.00E+00	0	0
0.5	9.96E-01	0.00E+00	0	0
0.5	9.96E-01	0.00E+00	0	0
‑‑‑‑‑‑‑‑‑‑				

#4 110 m tower

r	m	x_cg	y_cg	ri_x	ri_y	x_sh	y_sh	E	G

$1 50 110 m tower

r	m	x_cg	y_cg	ri_x	ri_y	x_sh	y_sh	E	G
0	4.54E+03	0	0	2.13E+00	2.13E+00	0	0	2.10E+11	8.08E+10
2.2446	4.48E+03	0	0	2.11E+00	2.11E+00	0	0	2.10E+11	8.08E+10
4.4893	4.41E+03	0	0	2.10E+00	2.10E+00	0	0	2.10E+11	8.08E+10
6.7339	4.35E+03	0	0	2.08E+00	2.08E+00	0	0	2.10E+11	8.08E+10
8.9786	4.29E+03	0	0	2.06E+00	2.06E+00	0	0	2.10E+11	8.08E+10
11.2232	4.22E+03	0	0	2.04E+00	2.04E+00	0	0	2.10E+11	8.08E+10
13.4679	4.16E+03	0	0	2.03E+00	2.03E+00	0	0	2.10E+11	8.08E+10
15.7125	4.10E+03	0	0	2.01E+00	2.01E+00	0	0	2.10E+11	8.08E+10
17.9572	4.04E+03	0	0	1.99E+00	1.99E+00	0	0	2.10E+11	8.08E+10
20.2018	3.98E+03	0	0	1.97E+00	1.97E+00	0	0	2.10E+11	8.08E+10
22.4465	3.92E+03	0	0	1.96E+00	1.96E+00	0	0	2.10E+11	8.08E+10
24.6911	3.86E+03	0	0	1.94E+00	1.94E+00	0	0	2.10E+11	8.08E+10
26.9358	3.80E+03	0	0	1.92E+00	1.92E+00	0	0	2.10E+11	8.08E+10
29.1804	3.74E+03	0	0	1.90E+00	1.90E+00	0	0	2.10E+11	8.08E+10
31.4251	3.68E+03	0	0	1.89E+00	1.89E+00	0	0	2.10E+11	8.08E+10
33.6697	3.62E+03	0	0	1.87E+00	1.87E+00	0	0	2.10E+11	8.08E+10
35.9144	3.56E+03	0	0	1.85E+00	1.85E+00	0	0	2.10E+11	8.08E+10
38.159	3.51E+03	0	0	1.83E+00	1.83E+00	0	0	2.10E+11	8.08E+10
40.4037	3.45E+03	0	0	1.82E+00	1.82E+00	0	0	2.10E+11	8.08E+10
42.6483	3.39E+03	0	0	1.80E+00	1.80E+00	0	0	2.10E+11	8.08E+10
44.893	3.34E+03	0	0	1.78E+00	1.78E+00	0	0	2.10E+11	8.08E+10
47.1376	3.28E+03	0	0	1.76E+00	1.76E+00	0	0	2.10E+11	8.08E+10
49.3822	3.22E+03	0	0	1.75E+00	1.75E+00	0	0	2.10E+11	8.08E+10
51.6269	3.17E+03	0	0	1.73E+00	1.73E+00	0	0	2.10E+11	8.08E+10
53.8715	3.12E+03	0	0	1.71E+00	1.71E+00	0	0	2.10E+11	8.08E+10
56.1162	3.06E+03	0	0	1.70E+00	1.70E+00	0	0	2.10E+11	8.08E+10
58.3608	3.01E+03	0	0	1.68E+00	1.68E+00	0	0	2.10E+11	8.08E+10
60.6055	2.96E+03	0	0	1.66E+00	1.66E+00	0	0	2.10E+11	8.08E+10
62.8501	2.90E+03	0	0	1.64E+00	1.64E+00	0	0	2.10E+11	8.08E+10
65.0948	2.85E+03	0	0	1.63E+00	1.63E+00	0	0	2.10E+11	8.08E+10
67.3394	2.80E+03	0	0	1.61E+00	1.61E+00	0	0	2.10E+11	8.08E+10
69.5841	2.75E+03	0	0	1.59E+00	1.59E+00	0	0	2.10E+11	8.08E+10
71.8287	2.70E+03	0	0	1.57E+00	1.57E+00	0	0	2.10E+11	8.08E+10
74.0734	2.65E+03	0	0	1.56E+00	1.56E+00	0	0	2.10E+11	8.08E+10
76.318	2.60E+03	0	0	1.54E+00	1.54E+00	0	0	2.10E+11	8.08E+10
78.5627	2.55E+03	0	0	1.52E+00	1.52E+00	0	0	2.10E+11	8.08E+10
80.8073	2.50E+03	0	0	1.50E+00	1.50E+00	0	0	2.10E+11	8.08E+10
83.052	2.45E+03	0	0	1.49E+00	1.49E+00	0	0	2.10E+11	8.08E+10
85.2966	2.40E+03	0	0	1.47E+00	1.47E+00	0	0	2.10E+11	8.08E+10
87.5413	2.36E+03	0	0	1.45E+00	1.45E+00	0	0	2.10E+11	8.08E+10
89.7859	2.31E+03	0	0	1.43E+00	1.43E+00	0	0	2.10E+11	8.08E+10
92.0306	2.26E+03	0	0	1.42E+00	1.42E+00	0	0	2.10E+11	8.08E+10
94.2752	2.22E+03	0	0	1.40E+00	1.40E+00	0	0	2.10E+11	8.08E+10
96.5198	2.17E+03	0	0	1.38E+00	1.38E+00	0	0	2.10E+11	8.08E+10
98.7645	2.13E+03	0	0	1.36E+00	1.36E+00	0	0	2.10E+11	8.08E+10
101.0091	2.08E+03	0	0	1.35E+00	1.35E+00	0	0	2.10E+11	8.08E+10
103.2538	2.04E+03	0	0	1.33E+00	1.33E+00	0	0	2.10E+11	8.08E+10
105.4984	1.99E+03	0	0	1.31E+00	1.31E+00	0	0	2.10E+11	8.08E+10
107.7431	1.95E+03	0	0	1.29E+00	1.29E+00	0	0	2.10E+11	8.08E+10
109.9877	1.91E+03	0	0	1.28E+00	1.28E+00	0	0	2.10E+11	8.08E+10

l_x	l_y	l_p	k_x	k_y	A	pitch	x_e	y_e
2.58E+00	2.58E+00	5.16E+00	0.5	0.5	5.68E-01	0	0	0
2.50E+00	2.50E+00	5.00E+00	0.5	0.5	5.60E-01	0	0	0
2.42E+00	2.42E+00	4.85E+00	0.5	0.5	5.52E-01	0	0	0
2.35E+00	2.35E+00	4.70E+00	0.5	0.5	5.44E-01	0	0	0
2.28E+00	2.28E+00	4.55E+00	0.5	0.5	5.36E-01	0	0	0
2.21E+00	2.21E+00	4.41E+00	0.5	0.5	5.28E-01	0	0	0
2.14E+00	2.14E+00	4.27E+00	0.5	0.5	5.20E-01	0	0	0
2.07E+00	2.07E+00	4.14E+00	0.5	0.5	5.12E-01	0	0	0
2.00E+00	2.00E+00	4.00E+00	0.5	0.5	5.05E-01	0	0	0
1.94E+00	1.94E+00	3.87E+00	0.5	0.5	4.97E-01	0	0	0
1.87E+00	1.87E+00	3.75E+00	0.5	0.5	4.90E-01	0	0	0
1.81E+00	1.81E+00	3.62E+00	0.5	0.5	4.82E-01	0	0	0
1.75E+00	1.75E+00	3.50E+00	0.5	0.5	4.75E-01	0	0	0
1.69E+00	1.69E+00	3.39E+00	0.5	0.5	4.67E-01	0	0	0
1.64E+00	1.64E+00	3.27E+00	0.5	0.5	4.60E-01	0	0	0
1.58E+00	1.58E+00	3.16E+00	0.5	0.5	4.53E-01	0	0	0
1.53E+00	1.53E+00	3.05E+00	0.5	0.5	4.45E-01	0	0	0
1.47E+00	1.47E+00	2.95E+00	0.5	0.5	4.38E-01	0	0	0
1.42E+00	1.42E+00	2.85E+00	0.5	0.5	4.31E-01	0	0	0
1.37E+00	1.37E+00	2.75E+00	0.5	0.5	4.24E-01	0	0	0
1.32E+00	1.32E+00	2.65E+00	0.5	0.5	4.17E-01	0	0	0
1.28E+00	1.28E+00	2.55E+00	0.5	0.5	4.10E-01	0	0	0
1.23E+00	1.23E+00	2.46E+00	0.5	0.5	4.03E-01	0	0	0
1.19E+00	1.19E+00	2.37E+00	0.5	0.5	3.96E-01	0	0	0
1.14E+00	1.14E+00	2.28E+00	0.5	0.5	3.89E-01	0	0	0
1.10E+00	1.10E+00	2.20E+00	0.5	0.5	3.83E-01	0	0	0
1.06E+00	1.06E+00	2.12E+00	0.5	0.5	3.76E-01	0	0	0
1.02E+00	1.02E+00	2.04E+00	0.5	0.5	3.69E-01	0	0	0
9.80E-01	9.80E-01	1.96E+00	0.5	0.5	3.63E-01	0	0	0
9.42E-01	9.42E-01	1.88E+00	0.5	0.5	3.56E-01	0	0	0
9.05E-01	9.05E-01	1.81E+00	0.5	0.5	3.50E-01	0	0	0
8.69E-01	8.69E-01	1.74E+00	0.5	0.5	3.44E-01	0	0	0
8.35E-01	8.35E-01	1.67E+00	0.5	0.5	3.37E-01	0	0	0
8.01E-01	8.01E-01	1.60E+00	0.5	0.5	3.31E-01	0	0	0
7.69E-01	7.69E-01	1.54E+00	0.5	0.5	3.25E-01	0	0	0
7.37E-01	7.37E-01	1.47E+00	0.5	0.5	3.19E-01	0	0	0
7.06E-01	7.06E-01	1.41E+00	0.5	0.5	3.12E-01	0	0	0
6.77E-01	6.77E-01	1.35E+00	0.5	0.5	3.06E-01	0	0	0
6.48E-01	6.48E-01	1.30E+00	0.5	0.5	3.00E-01	0	0	0
6.20E-01	6.20E-01	1.24E+00	0.5	0.5	2.95E-01	0	0	0
5.94E-01	5.94E-01	1.19E+00	0.5	0.5	2.89E-01	0	0	0
5.68E-01	5.68E-01	1.14E+00	0.5	0.5	2.83E-01	0	0	0
5.42E-01	5.42E-01	1.08E+00	0.5	0.5	2.77E-01	0	0	0
5.18E-01	5.18E-01	1.04E+00	0.5	0.5	2.71E-01	0	0	0
4.95E-01	4.95E-01	9.89E-01	0.5	0.5	2.66E-01	0	0	0
4.72E-01	4.72E-01	9.44E-01	0.5	0.5	2.60E-01	0	0	0
4.50E-01	4.50E-01	9.00E-01	0.5	0.5	2.55E-01	0	0	0
4.29E-01	4.29E-01	8.58E-01	0.5	0.5	2.49E-01	0	0	0
4.08E-01	4.08E-01	8.17E-01	0.5	0.5	2.44E-01	0	0	0
3.89E-01	3.89E-01	7.78E-01	0.5	0.5	2.38E-01	0	0	0

C.2   Main input

Input HAWCStab2
begin new_htc_structure;
;
  begin main_body;   tower 110m
   name   tower ;
   type   timoschenko ;
   nbodies   1 ;
   node_distribution   c2_def ;
   damping   5.0E-02 5.0E-02 8.0E-01 1.0E-03 1.0E-03 4.5E-04 ;
   concentrated_mass 10 0.0 1.9 0.0 2.539E5 9.126E5 9.126E5 1E5 ;
   begin timoschenko_input;
    filename ./data/hawc_Sigrid1.nrl ;
    set 4 1 ;
   end timoschenko_input;
   begin c2_def;   Definition of centerline (main_body coordinates)
    nsec 10;
    sec 1 0.0 0.0 0.0   0.0 ; x y z twist
    sec 2 0.0 0.0 -12.22 0.0 ;
    sec 3 0.0 0.0 -24.44 0.0 ;
    sec 4 0.0 0.0 -36.66 0.0 ;
    sec 5 0.0 0.0 -48.88 0.0 ;
    sec 6 0.0 0.0 -61.11 0.0 ;
    sec 7 0.0 0.0 -73.33 0.0 ;
    sec 8 0.0 0.0 -85.55 0.0 ;
    sec 9 0.0 0.0 -97.77 0.0 ;
    sec 10 0.0 0.0 -110 0.0 ;
   end c2_def ;
  end main_body;
;
  begin main_body;
   name   shaft ;
   type   timoschenko ;
   nbodies   1 ;
   node_distribution   c2_def ;
   damping   3.0e-05 3.0e-05 4.0e-02 3.0e-07 3.0e-07 4.5e-03 ;
   concentrated_mass 1 0.0 0.0 0.0 10.0 1E5 1E5 5.026E6 ;
   begin timoschenko_input;
    filename ./data/hawc_Sigrid1.nrl ;
    set 2 1 ;   set subset
   end timoschenko_input;
   begin c2_def;   Definition of centerline (main_body coordinates)
    nsec 5;
    sec 1 0.0 0.0 0.0   0.0 ; Tower top x y z twist
    sec 2 0.0 0.0 0.1   0.0 ; Generator end
    sec 3 0.0 0.0 1.96256 0.0 ; Gearbox position
    sec 4 0.0 0.0 3.10710 0.0 ; Main bearing
    sec 5 0.0 0.0 5.01910 0.0 ; rotor centre
   end c2_def ;
  end main_body;
;
  begin main_body;   nei
   name hub1 ;
   type timoschenko ;

```
    nbodies 1 ;
    node_distribution uniform 2 ;
    damping 2.00E-04 2.00E-04 2.00E-03 3.00E-05 3.00E-05 2.00E-04 ;
;   damping 2.00 2.00 2.00 3.00 3.00 2.00 ;
    begin timoschenko_input;
     filename ./data/hawc_Sigrid1.nrl ;
     set 3 3 ;
    end timoschenko_input;
    begin c2_def; Definition of centerline (main_body coordinates)
     nsec 4;
     sec 1 0.00E+00 0.00E+00 0.00E+00 0.00E+00 ; x y z twist
     sec 2 0.00E+00 0.00E+00 1.00E+00 0.00E+00 ;
     sec 3 0.00E+00 0.00E+00 2.00E+00 0.00E+00 ;
     sec 4 0.00E+00 0.00E+00 2.46710 0.00E+00 ;
    end c2_def ;
 end main_body;
;
 begin main_body;
  name hub2 ;
  copy_main_body hub1;
 end main_body;
;
 begin main_body;
  name hub3 ;
  copy_main_body hub1;
 end main_body;
;
 begin main_body; nei
  name      blade1 ;
  type      timoschenko ;
  nbodies    9 ;
  node_distribution    c2_def ;
  begin timoschenko_input;
   filename ./data/hawc_Sigrid1.nrl ;
   set 1 1 ;          set subset
  end timoschenko_input;
  begin c2_def;          Definition of centerline (main_body coordinates)
   nsec 21;
          sec              1          0          0          0 -1.36E+01; xyz twist
          sec              2 -7.22E-02          0 1.38E+00 -1.35E+01; xyz twist
          sec              3 -2.84E-01          0 4.29E+00 -1.32E+01; xyz twist
          sec              4 -5.06E-01          0 7.21E+00 -1.26E+01; xyz twist
          sec              5 -7.05E-01          0 1.01E+01 -1.18E+01; xyz twist
          sec              6 -9.12E-01          0 1.45E+01 -1.03E+01; xyz twist
          sec              7 -9.90E-01          0 1.89E+01 -8.83E+00; xyz twist
          sec              8 -1.01E+00          0 2.28E+01 -7.60E+00; xyz twist
          sec              9 -9.77E-01          0 2.76E+01 -6.27E+00; xyz twist
          sec             10 -9.48E-01          0 3.01E+01 -5.68E+00; xyz twist
          sec             11 -8.75E-01          0 3.49E+01 -4.65E+00; xyz twist    50%blade
          sec             12 -7.94E-01          0 3.98E+01 -3.77E+00; xyz twist
          sec             13 -7.18E-01          0 4.47E+01 -3.01E+00; xyz twist
          sec             14 -6.49E-01          0 4.95E+01 -2.34E+00; xyz twist
          sec             15 -6.18E-01          0 5.20E+01 -2.03E+00; xyz twist
```

```
              sec            16  -5.91E-01      0   5.44E+01 -1.72E+00; xyz twist
              sec            17  -5.70E-01      0   5.64E+01 -1.47E+00; xyz twist
              sec            18  -5.08E-01      0   6.05E+01 -9.64E-01; xyz twist
              sec            19  -4.08E-01      0   6.46E+01 -4.50E-01; xyz twist
            sec 20  -3.08E-01  0.000  6.67E+01   -1.83E-01;
            sec 21       -1.84E-01 0.000  6.80E+01   0.000;
      end c2_def ;
    end main_body;
;
   begin main_body;
     name         blade2 ;
     copy_main_body blade1;
   end main_body;
;
   begin main_body;
     name         blade3 ;
     copy_main_body blade1 ;
   end main_body;
;
   begin orientation;
;
     begin base;
       body   tower;
       inipos     0.0 0.0 0.0 ;       initial position of node 1
       body_eulerang 0.0 0.0 0.0;
     end base;
;
     begin relative;
       body1  tower last;
       body2  shaft 1;
       body2_eulerang 90.0 0.0 0.0;
       body2_eulerang 5.0 0.0 0.0;   5 deg tilt
     end relative;
;
     begin relative;
       body1  shaft last;
       body2  hub1 1;
       body2_eulerang -90.0 0.0 0.0;
       body2_eulerang 2.0 0.0 0.0;     2.0 deg cone
     end relative;
;
     begin relative;
       body1  shaft last;
       body2  hub2 1;
       body2_eulerang -90.0 0.0 0.0;
       body2_eulerang 0.0 -120.0 0.0;
       body2_eulerang 2.0 0.0 0.0;     2.0 deg cone
     end relative;
;
     begin relative;
       body1  shaft last;
       body2  hub3 1;
       body2_eulerang -90.0 0.0 0.0;
```

```
      body2_eulerang 0.0 120.0 0.0;
      body2_eulerang 2.0 0.0 0.0;     2.0 deg cone
     end relative;
;
    begin relative;
     body1  hub1 last;
     body2  blade1 1;
     body2_eulerang 0.0 0.0 0.0;
    end relative;
;
    begin relative;
     body1  hub2 last;
     body2  blade2 1;
     body2_eulerang 0.0 0.0 0.0;
    end relative;
;
    begin relative;
     body1  hub3 last;
     body2  blade3 1;
     body2_eulerang 0.0 0.0 0.0;
    end relative;
  end orientation;
 ;----------------------------------------------------------------
 begin constraint;
   begin fix0;  fixed to ground in translation and rotation of node 1
    body tower;
   end fix0;
;
    begin bearing1;                free bearing
     name  shaft_rot ;
     body1 tower last;
     body2 shaft 1;
     bearing_vector 2 0.0 0.0 -1.0;    vector in body2 coordinates where the free rotation is present
    end bearing1;
;
    begin fix1;
     body1 shaft last;
     body2 hub1 1;
    end fix1;
;
    begin fix1;
     body1 shaft last;
     body2 hub2 1;
    end fix1;
;
    begin fix1;
     body1 shaft last;
     body2 hub3 1;
    end fix1;
;
    begin bearing2;              forced bearing
     name pitch1;
     body1 hub1 last;
```

```
      body2 blade1 1;
      bearing_vector 2 0.0 0.0 -1.0;   vector in body2 coordinates where the free rotation is present
    end bearing2;
;
    begin bearing2;              forced bearing
     name pitch2;
     body1 hub2 last;
     body2 blade2 1;
     bearing_vector 2 0.0 0.0 -1.0;  vector in body2 coordinates where the free rotation is present
    end bearing2;
;
    begin bearing2;              forced bearing
     name pitch3;
     body1 hub3 last;
     body2 blade3 1;
     bearing_vector 2 0.0 0.0 -1.0;  vector in body2 coordinates where the free rotation is present
    end bearing2;
  end constraint;
;;
end new_htc_structure;
;
begin hawcstab2 ;
  begin ground_fixed_substructure ;
   main_body tower ;
   log_decrements 2.0 2.0 ;
  end ground_fixed_substructure ;
;
  begin rotating_axissym_substructure ;
   main_body shaft ;
   log_decrements 5.0 ;
  end rotating_axissym_substructure ;
;
  begin rotating_threebladed_substructure ;
   main_body hub1 ;
   main_body blade1 ;
   log_decrements 1.8 2.2  ;
  end rotating_threebladed_substructure ;
;
  operational_data_filename ./data/op_Sigrid2.opt ;
end hawcstab2 ;
;
begin wind ;
  density          1.225 ; to be checked
  wsp            15;
  tint         0.0 ;
  horizontal_input    1   ;      0=false  1=true
  windfield_rotations   0.0  0.0 0.0 ;   yaw  tilt  rotation
  center_pos0        0.0 0.0 -110.0 ;
  shear_format       1 0 ;0=none 1=constant 2=log 3=power 4=linear
  turb_format        0   ; 0=none  1=mann 2=flex
  tower_shadow_method   0   ; 0=none  1=potential flow 2=jet
;
end wind;
```

```
;
begin aero ;
 nblades  3;
 hub_vec shaft -3 ;        rotor rotation vector
 link 1 mbdy_c2_def blade1;
 link 2 mbdy_c2_def blade2;
 link 3 mbdy_c2_def blade3;
 ae_filename      ./data/Sigrid1_ae.nrl;
  pc_filename      ./data/hawc_pc.nrl;
 induction_method  1 ;   0=none  1=normal
 aerocalc_method   1 ;   0=ingen aerodynamic  1=med aerodynamic
 aerosections    40 ;
 ae_sets       1 1 1;
 tiploss_method   1 ;   0=none  1=prandtl
 dynstall_method   2 ;   0=none  1=stig øye method 2=mhh method
end aero ;
;
exit;
```